DEVELOPMENT OF ZnO/SiO_2 PHOTOCATALYSTS FOR ESTERIFICATION OF WASTE COOKING OIL

BY

OLORUNTOBA ORIOLOWO

DEPARMENT OF CHEMICAL ENGINEERING,

AHMADU BELLO UNIVERSITY, ZARIA

NIGERIA

JUNE, 2016

DEVELOPMENT OF ZnO/SiO_2 PHOTOCATALYSTS FOR ESTERIFICATION OF WASTE COOKING OIL

By

Oloruntoba ORIOLOWO, B.Eng (FUT Minna, 2010)
(MSc/Eng/27632/2012-2013)

A DISSERTATION SUBMITTED TO THE SCHOOL OF POSTGRADUATE STUDIES,
AHMADU BELLO UNIVERSITY, ZARIA

IN PARTIAL FULFILLMENT OF THE REQUIREMENTS FOR THE AWARD OF A
MASTER OF SCIENCE DEGREE IN CHEMICAL ENGINEERING.

DEPARTMENT OF CHEMICAL ENGINEERING,
FACULTY OF ENGINEERING,
AHMADU BELLO UNIVERSITY, ZARIA
NIGERIA.

JUNE, 2016

DECLARATION

I declare that the work in this dissertation titled "DEVELOPMENT OF ZnO/SiO_2 PHOTOCATALYST FOR ESTERIFICATION OF WASTE COOKING OIL" was carried out by me in the Department of Chemical Engineering, Ahmadu Bello University, Zaria, under the supervision of Dr. Abdulhamid Hamza and Dr. Bello Mukhtar of the Department of Chemical Engineering, Ahmadu Bello University, Zaria. The information derived from the literature has been duly acknowledged in the text and a list of reference provided. No part of this dissertation was previously presented for another degree in this University or any other Institution.

_____ _____

Signature Date

CERTIFICATION

This dissertation entitled "**DEVELOPMENT OF ZnO/SiO_2 PHOTOCATALYST FOR ESTERIFICATION OF WASTE COOKING OIL**" by Oloruntoba ORIOLOWO, meets the regulations governing the award of the degree of Master of Science (M.Sc) of the Ahmadu Bello University, and is approved for its contribution to knowledge and literary presentation.

_____ _____

Dr. Abdulhamid Hamza Date

Chairman, Supervisory Committee

_____ _____

Dr. Bello Mukhtar Date

Member, Supervisory Committee

_____ _____

Dr. S.M. Waziri Date

Head, Dept. of Chemical Engineering

_____ _____

Prof. Kabir Bala Date

Dean, School of Postgraduate Studies

DEDICATION

This M.Sc dissertation work is dedicated to my beloved parents, siblings, and my unborn children.

ACKNOWLEDGEMENTS

First and foremost, all praise, thanks and adorations to the Almighty God, the creator of the universe for sustaining me to accomplish this degree programme. Without His limitless grace and mercies, this work would not have been realized. For the success of this work and His countless blessings upon my life, I will forever praise Him.

My profound gratitude goes to my supervisor Dr. Abdulhamid Hamza for his cordial relationship, continued support, tremendous help, encouragement, pieces of advice and guidance he rendered throughout this programme, I am grateful sir. Special thanks to Dr. Bello Mukhtar who is also part of the supervisory committee of this work, for his gentle and firm corrections. God will continue to shower His blessings to you sir. My heartfelt appreciation goes to both academic and non-academic staff of the Department of Chemical Engineering, Ahmadu Bello University, Zaira for their constructive criticism and technical inputs that made this research a success.

To all my friends and colleagues: Seyi, Gbenga, Anthony, Gold, Umar, Joke, Aisha, Oyin, Funke, David, Sherrif, Gman, Moshood, Toba, Zanna, Abdul, Bugaje, Mukhtar, Mr. Y, Abudraulf, Tomi, Kate, Hajia and those I forget to mention their name, I say a big thank for your immensurable contribution in one way or the other.

Finally, I sincerely render my appreciation to all my family members: my parents, siblings (D1, Dammy, and Seye), uncles and aunts as well as my cousins for their prayers, encouragement and special support throughout my education pursuits at ABU, Zaira.

May God continually cause His light to shine ahead of you all and bless you in all endeavors of life, Amen. Once again, thank you all.

ABSTRACT

Waste cooking oil (WCO) as a feedstock used for biodiesel production is recognized as an attractive alternative to vegetable oil. However, the high concentration of free fatty acid (FFA) coupled with other impurities in WCO may require several pretreatments prior to transesterification. This study explored a novel method of estrifying WCO by employing a photocatalytic process using ZnO/SiO_2 as the catalyst. The developed catalysts with various proportions of ZnO loading onto the silica support (10-ZnO/SiO_2, 20-ZnO/SiO_2, 30-ZnO/SiO_2 and 40-ZnO/SiO_2) were synthesized by mechanochemical method followed by solid state dispersion. It was characterized using X-Ray Diffraction (XRD), X-ray Fluorescence Spectroscopy (XRF), Scanning Electron Microscopy (SEM), pH at point of zero charge (pH_{PZC}) and Specific Surface Area Analysis. The composition of the raw and esterified WCO was analyzed using Gas chromatography Mass spectrometry (GC-MS) technique. The photocatalytic activity of the synthesized catalysts was studied by monitoring the kinetics of degradation of methylene blue (MB) and benzoic acid (BA) under solar irradiation. The percentage FFA conversion in WCO for the developed catalysts in the order 10-ZnO/SiO_2, 20-ZnO/SiO_2, 30-ZnO/SiO_2 and 40-ZnO/SiO_2 was 76.4, 79.9, 81.5, and 90.3 in the dark (6 hr) and 78.7, 82.0, 84.10, 94.0 after irradiation time of 4 hours, with 40-ZnO/SiO_2 having the highest percentage FFA conversion. The GC-MS results revealed that more esters were being formed in the presence of light than in the dark with no occurrence of soap formation during the photocatalytic esterification process.

TABLE OF CONTENT

LIST OF FIGURES

LIST OF TABLES

LIST OF PLATES

LIST OF ABBREVIATIONS

AOP	Advanced Oxidation Process
BA	Benzoic acid
CWA	Chemical Warfare Agent
EU	European Union
FFA	Free Fatty Acid
GC-MS	Gas Chromatograph Mass Spectrometry
hr	Hour
ISO	International Standard of Organization
JCPDS	Joint Committee on Powder Diffraction Standard
K_{app}	Apparent Rate Constant
MB	Methylene blue
min	Minute
nm	Nanometer
NGRL	National Geological Research Laboratory
PCA	Photocatalytic Activity
pH_{PZC}	pH at Point of Zero Charge
PTDF	Petroleum Training Development Fund
SEM	Scanning Electron Microscopy
SC	Semiconductor
SiO_2	Silica
UV	Ultraviolet
WCO	Waste Cooking Oil
W	Watt
XRD	X-Ray Diffraction

ZnO	Zinc oxide
θ	Diffraction angle (^{o})
λ_{max}	Maximum Wavelength

CHAPTER ONE

INTRODUCTION

1.1 Preamble

The production of green fuels is attracting, generating increasing academic and industrial interests. Biodiesel is one of the green fuels that has many advantages such as low emission of carbon dioxide, biodegradability and good lubricating properties (Jacobson *et al.,* 2008). Biodiesel consists of alkyl esters derived from either the transesterification of triglycerides in oils and fats, or the esterification of free fatty acids (FFA) with short-chained alcohols.

Utilization of high FFA feeds in traditional biodiesel production processes leads to depletion of the catalysts, as well as increased purification costs, because the FFA is saponified by the homogeneous base catalyst, producing excess soap (Zheng *et al.,* 2006). Esterification of free fatty acids to yield alky esters in the presence of an acidic catalyst is the conventional route to reduce FFA of oils used in biodiesel production. Esterification is commonly carried out in a homogeneous phase in the presence of acid catalysts because of its high conversion efficiency and lower cost (Carmo Jr *et al.,* 2009). However, the use of the homogenous acid catalyst has some drawbacks such as effluent disposal problem, corrosion, loss of catalyst, and high amount of base required for neutralization of the effluent (Srilatha *et al.,* 2009). In view of these setbacks, heterogeneous catalysts have been considered as an alternative to minimize environmental damage and reduce biodiesel cost.

There are several works on the production of heterogeneous catalysts using mesoporous sulfonic acid (Mbaraka and Shanks, 2006), sulfonated carbons (Liu *et al.,* 2008), modified zirconias (Lopez *et al.,* 2008), zeolite (Chang *et al.,* 2008), heteropoly acid-based catalysts (Xu *et al.,* 2009), ion exchange resin (Gan *et al.,* 2012), and copper oxide supported on carbon catalyst

(Ong *et al.,* 2014) for the esterification of high FFA oils used in biodiesel production. Despite several studies carried out on heterogeneous catalyst, few works have been performed on FFA esterification by a heterogeneous photocatalytic process (Corro *et al*., 2013; Kiwngam and Wanchai, 2014). Focus of Corro *et al* (2013) was mainly on the photocatalytic esterification of *Jatropha curcas crude oil* under UV irradiation catalyzed by ZnO/SiO_2 photocatalyst. Using visible light irradiation and varying the proportion of ZnO content unto the catalyst support was not reported. Heterogeneous photocatalysis has many advantages over thermal catalytic processes because it can be performed at room temperature and atmospheric pressure using direct solar energy or artificial light sources. It is environmental friendly and enables reusability of the catalyst which minimizes its consumption and cost of treatment (Corro *et al.,* 2013).

Zinc oxide (ZnO) nanoparticles have been extensively used as a heterogeneous photocatalyst for the degradation of various organic pollutants in water and air under ultraviolent irradiation. ZnO is interesting because it is easy to prepare, and harmless to the environment. Though the FFA could be photocatalytically-esterified using ZnO alone, a technical problem arises with its use due to a strong disaggregation of the solid in the reacting mixture. Also, separation of ZnO particles and the liquid phase is a difficult task and a high content of fine ZnO particles will remain in the final esterified mixture (Corro *et al.,* 2013). Modification of ZnO supported on silica is very imperative because ZnO is unstable in acid conditions and shows rapid deactivation in bulk use due to aggregation (Mihai *et al.,* 2010). The silica obtained from Kankara kaolin may lower the band gap of ZnO due to the presence of impurities.

Thus, this work focuses on heterogeneous photocatalysis as an alternative method of treating FFA in waste cooking oil (WCO) for biodiesel production. The photocatalysts (ZnO and ZnO supported on silica) were synthesized by mechanochemical method using high energy ball

milling machine followed by solid state dispersion method. The photocatalysts were characterized using XRF, XRD, SEM, drift method for point of zero charge and Sear's method for specific surface area. The photocatalytic activity was initially evaluated using methylene blue (MB) and benzoic acid as model substrate under solar irradiation as prescribed by International Standard Organization (ISO) of evaluating the activity of photocatalysts. The synthesized photocatalysts were then applied for the reduction of FFA in WCO.

1.2 Research Problem Statement

Conventional esterification process (homogeneous and heterogeneous catalysis) employed as a pre - treatment for biodiesel production has been associated with high catalyst and energy consumption (via thermal heating method) leading to high biodiesel production cost.

1.3 Aim and Objectives

The aim of this research work is to develop ZnO/SiO_2 photocatalyst for the esterification of Waste Cooking Oil (WCO) as a pre-treatment step in biodiesel production.

The specific objectives are:

i. To synthesize ZnO and ZnO/SiO_2 photocatalysts using mechanochemical method followed by solid state dispersion.
ii. To characterize the composites using XRD, XRF, SEM, surface area, and point of zero charge (pH_{PZC}) analysis.
iii. To evaluate the photocatalytic activity of the synthesized photocatalysts using MB and benzoic acid as model substrate.
iv. To esterify free fatty acids present in waste cooking oil using the synthesized catalysts under visible light illumination.

1.4 Research Justification

i. The precursor materials for the production of ZnO/SiO_2 are readily available.

ii. Heterogeneous photocatalysis can be carried out at room temperature using light (solar) energy, thereby reducing operating cost.

iii. Utilization of waste cooking oil for biodiesel will add value to it and reduce environmental pollution.

1.5 Scope of Research

Synthesis, characterization and application of ZnO/SiO_2 photocatalysts in various ratios (10-ZnO/SiO_2, 20-ZnO/SiO_2, 30-ZnO/SiO_2, and 40-ZnO/SiO_2) for esterification of waste cooking oil under visible light irradiation

CHAPTER TWO

LITERATURE REVIEW

2.1 Potential Biodiesel Production Feedstocks

The conventional feedstocks for producing biodiesel are edible vegetable oils such as soyabean oil (Xie and Huang, 2006), sunflower oil (Turkan and Kalay, 2006) and palm oil (Hameed *et al*., 2009). More than 95% of the global production of biodiesel uses edible vegetable oil as feedstock (Balat and Balat, 2010). Biodiesel produced from edible vegetable oil is sometimes referred to as a first generation biofuel (Tariq *et al.,* 2012).

The cost of producing biodiesel is much higher than convection fuel, particularly when refined oil is used due to the high cost of the raw material. Haas *et al* (2006) developed economic model to estimate biodiesel production cost with soyabean oil as the raw material and they found that the cost of vegetable oil accounts for 82% of the total cost of biodiesel production. The remaining cost components were chemicals (7%), depreciation (5%), direct labour (2%) and general overhead (1%).

In addition, there are ethical concerns with respect to the use of potential food source as a fuel. In order to overcome ethical concerns with using a potential food source as fuel, the use of non-edible oils has also been investigated. Among the non-edible oils for biodiesel production were *Jatropha curcas crude oil* (Corro *et al.,* 2013), and rubber seed oil (Ong *et al.,* 2014). Although, *Jatropha curcas* plant can grow in poor quality soil and is often used for erosion control but growing this type of crop can still contribute to environmental damage and competition with food growing resources (Hara, 2009; Corro *et al.,* 2013). Meanwhile, this type of fuel is sometimes referred to as a second generation biodiesel (Tariq *et al.,* 2012).

Also, animal fats have been investigated for the production of biodiesel. Animal fat, however, has its own disadvantage when used for producing biodiesel. Because it contains high amounts of saturated fat, biodiesel produced from this feedstock tends to gel, limiting widespread application of this type of fuel particularly for winter-time use (Wen *et al.,* 2006).

More recently microalgae have been recognized as a potentially good source for biodiesel production because of their high oil content and rapid biomass production (Balat and Balat, 2010). Microalgae are sunlight – driven cell factories that convert carbon dioxide to potential biofuels and can be grown in a variety of aquatic environments. The cultivation of microalgae is currently not economically feasible due to the costs associated with harvesting the microalgae. Biodiesel from microalgae is sometimes called as third generation biodiesel (Tariq *et al.,* 2012).

2.1.1 Waste cooking oil (WCO)

The term "waste cooking oil" (WCO) refers to vegetable oil which has been used in food production and which is no longer viable for its intended use. Thus, someone's waste output is often someone else's raw material input. WCO arises from many different sources, including domestic, commercial and industrial. WCO is a potentially problematic waste stream which requires to be properly managed. The disposal of WCO can be problematic when disposed incorrectly, down kitchen sinks, where it can quickly cause blockages of sewer pipes when the oil solidifies. Properties of degraded WCO after it gets into sewage system are conducive to corrosion of metal and concrete elements. It also affects installations in waste water treatment plants. Thus, it adds to the cost of treating effluent or pollutes waterways (Szmigielski *et al.,* 2008).

The origin of WCO determines fatty acid compositions while history or duration that the oil was exposed to heat, food, and oxygen during cooking determines the oil's physical and chemical properties such as viscosity, water content, and FFA content. Oil degradation during cooking occurs through three main reactions: thermolytic, oxidative, and hydrolytic reactions (Issariyakul and Dalai, 2014). As a result of combination of these reactions during food preparation, various reaction derivatives are formed leading to an increase in polar content of the oil. It is advisable that used cooking oil should no longer be utilized for edible purpose when its polar content exceeds 25% (Kulkarni and Dalai, 2006). This concern has raised interests in utilizing used cooking oil as feedstock for biodiesel production.

Estimated amount of waste cooking oil (WCO) being generated in some countries has been reported (Carter *et al.,* 2005; Kulkarni and Dalai, 2006; Chhetri *et al.,* 2008). Unfortunately, published data from Sub-Saharan Africa is not available but the uniqueness of this work in Nigeria is that, it has a growing population of about 170 million people and as such, there is an increase in the rate at which fast food companies, restaurants and hotels are being set up. The large amount of WCO generated from these establishments on a daily basis can now be sold at a cheap price to biodiesel manufacturers.

2.2 Biodiesel Production

The methods for biodiesel production can be categorized into three types: these are chemical-catalytic (base or acid catalysis), bio-catalytic (enzyme catalysis) and non-catalytic processes. Several reviews of the different methods of biodiesel productions can be found in the literature (Marchetti *et al*., 2007). To date, most biodiesel processes use a soluble base as the catalyst in transesterification process, but the use of this catalyst complicates product recovery and purification. In 2007, around 19 biodiesel plants in EU member states were starting operations.

Currently, relatively large plants are found in Poland, Lithuania and Romania in addition to Germany and France (Leung *et al*., 2010). Solid or liquid catalysts are predominantly used in the two chemical catalytic processes (transesterification and pyrolysis) and in the case of the biological conversion the use of enzyme catalysis is employed. But out of these processes, transesterification is ascertained as most suitable method for the biodiesel production.

2.2.1 Transesterification process

Transesterification, also known as alcoholysis, is the conventional methodology for biodiesel production. It involves the displacement of alcohol from an ester by another alcohol in a process akin to hydrolysis, except that an alcohol is used instead of water as shown in Equation 2.1. The product of the reaction is a mixture of alky esters which are known as biodiesel and glycerol. This process has been extensively used to nosedive the viscosity of triglycerides. Meanwhile, it is a reversible reaction which proceeds essentially via the mixing of triglycerides and alcohols in the presence of a catalyst. Stoichiometrically, one mole of triglyceride requires three moles of alcohol in transesterification but in order to preclude reversible reaction to occur, excess alcohol is usually used to shift the equilibrium towards the formation of the esters, according to Le Chateliers principle. Many primary alcohols have been used for biodiesel production. These include methanol, ethanol, Isopropanol and butanol (Gerpen *et al*., 2004). The choice of which alcohol to use is determined by its cost, water content, case of recovery for recycle and the quantity required. High water content can lead to poor esterification reaction resulting in high yield of free fatty acids and soap. Methanol is most commonly used in transesterification mainly due to its economical benefits (Ma and Hann, 1999). Its choice can also be attributed to its short carbon chain length and less propensity to saponify thereby, increase the ester yield as well as

reduce consumption of the catalyst, when compared to other alcohols (Issariyakul *et al.*, 2006; Mendow *et al.*, 2011).

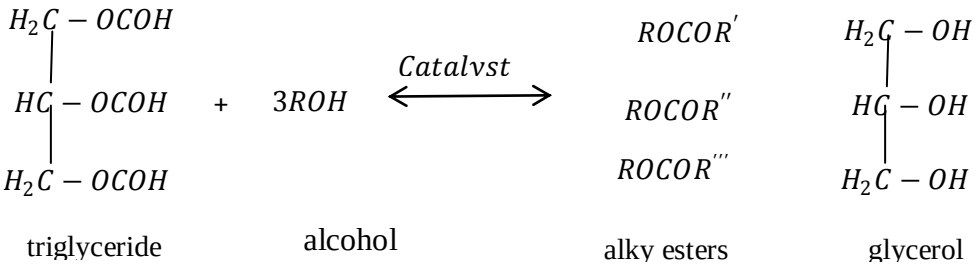

2.1

2.2.1.1 *Homogeneous transesterification*

Homogeneous base catalysis is most commonly used in commercial biodiesel production process because the process offers high yield in a short time with mild reaction conditions. Many researchers have reported that homogeneous base catalysis in transesterification is much faster than homogeneous acid catalysis (Freedman *et al.*, 1986). Homogeneous base catalysts such as NaOH, KOH, CH_3ONa or CH_3OK are used in the process. However, when these catalysts are used, feedstock selection is essential to the success and economic feasibility of biodiesel production because the catalysts require anhydrous conditions and low level of free fatty acid content in the feedstocks for the process to be effective. In a situation whereby feedstocks contain high free fatty acids and water content, homogeneous acid catalysis is more suitable. Although it requires a longer reaction time and a higher temperature than homogeneous base catalysis for the conversion process to be completed.

Saponification is one of the side reactions affecting the yield of biodiesel from vegetable oil. The production of soap, sometimes called alkaline hydrolysis, converts tri-alkylglycerols to glycerol and form a mixture of salts of long chain carboxylic acids. The saponification reaction of the catalyst (sodium hydroxide) and the FFA, forming soap and water is shown in Equation 2.2

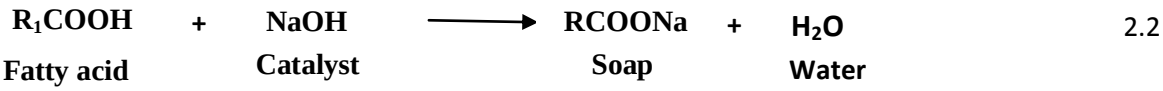

2.2

This reaction is undesirable because the soap lowers the yield of the biodiesel and inhibits the separation of the esters from the glycerol. In addition, it binds with the catalyst meaning that more catalyst will be needed and hence the process will involve a higher cost (Leung *et al*., 2010).

The biodiesel industry has dealt with the problem of saponification by replacing the hydroxides traditionally used as catalysts (KOH and NaOH) with methoxides (mainly CH_3ONa). Although this proceeding does not completely prevent saponification, using a methoxide catalyst can significantly reduce its occurrence. Additionally, some studies affirm that, provided the vegetable oil is refined, the yield loss resulting from the formation of soaps is sufficiently small to be neglected (Fonseca *et al*., 2010). Hence, in order to prevent the biodiesel yield loss due to the saponification reaction, oil and alcohol must be dry and the oil should have a minimum amount of free fatty acids (Macario *et al*., 2010).

2.2.1.2 Heterogeneous transesterification

Heterogeneous base catalysts have gained significant attraction from numerous biodiesel researchers. This is because the catalyst removal process is simple and does not create waste water that is generated during the catalyst removal step when homogeneous catalysts are used. In addition, heterogeneous catalyst can be regenerated and reused, rendering biodiesel production in a continuous process possible. However, the use of such catalyst is limited by free fatty acid usually contained in low quality feedstock such as Waste Cooking Oil. Common heterogeneous base catalysts such as MgO, CaO, SrO and BaO have been investigated by scientific community in order to catalyze transesterification (Liu, 1994).

2.2.1.3 *Enzymatic transesterification*

Enzymatic transesterification, especially those using lipase has drawn researchers' attention in the last ten years due to the downstream processing problem posed by chemical transesterification. Huge amount of wastewater generation and difficulty in glycerol recovery are among problems that eventually increase the overall biodiesel production cost and being not environment benign (Lam *et al.,* 2010).

In contrast, enzyme catalysis proceeds without the generation of by-products, easy recovery of product, mild reaction conditions, insensitive to high FFA oil and catalyst can be reused. These advantages prove that enzyme catalyzed biodiesel production has high potential to be an eco-friendly process and a promising alternative to the chemical process. However, it still has its fare share of constraints especially when implemented in industrial scale such as high cost of enzyme, slow reaction rate and enzyme deactivation (Lam *et al.,* 2010). The advantages and disadvantages of different types of catalysts used in transesterification of triglyceride oils can be studied in more detail in the review article of Lam *et al.,* (2010).

2.3 Esterification Process

Esterification is a pre-treatment step to reduce the levels of free fatty acids in the low cost feedstocks to an acceptable range, making the feedstocks suitable for further processing in the standard biodiesel synthesis. As a reversible reaction, it occurs by the reaction of carboxylic acids (fatty acids) and alcohols in the presence of catalyst, resulting in the formation of water and at least one ester product as shown in Equation 2.3. To enable biodiesel production from high FFA raw materials in a more cost effective way, the study of such reaction is necessary (Dias *et al.,* 2008).

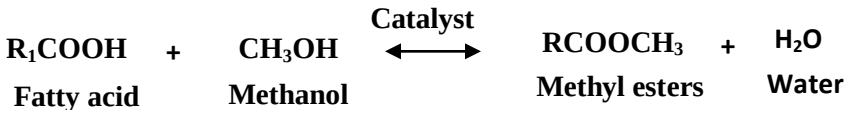

2.3

This side reaction is of great importance due not only to the possible increase on the biodiesel production, but also because it will affect the properties of future biodiesel (Marchetti *et al*., 2007a). In addition to transesterification of triglyceride, biodiesel can be produced from free fatty acids through esterification. Triglyceride is a type of ester and the reaction that converts triglyceride into biodiesel is known as transesterification (transforming ester). In contrast, free fatty acid is not an ester and therefore the reaction to produce biodiesel from FFA is called esterification which can be termed as making esters (Issariyakul and Dalai, 2014). Some conventional esterification processes are discussed in the next sub sections.

2.3.1 Homogeneous acid catalyzed esterification

In biodiesel production from feedstock containing high FFA and water content, acid catalysis is preferable. This approach can be used to avoid saponification and FFA is directly converted to ester through esterification while glycerides are converted to ester through transesterification. Therefore, acid catalysts can be used to catalyze both esterification and transesterification while base catalysts only catalyze transesterification but not esterification (Liu *et al.*, 1994). The disadvantages of homogeneous acid catalysis are that it requires a higher reaction temperature, an acid-tolerable reactor, and a longer reaction time due to slower rate of the reaction. Examples of homogeneous acid catalysts are H_2SO_4, H_3PO_4, HCl, and BF_3.

2.3.2 Heterogeneous acid catalyzed esterification

Heterogeneous acid catalysts are the most promising catalysts for biodiesel production and are expected to dominate commercial industries in the coming years. This is due to the simplicity in biodiesel purification step that eliminates waste water, reusability that make continuous process possible, and their ability to handle low quality feedstock with high FFA content via simultaneous esterification and transesterification. Heterogeneous acid catalysis, however, usually requires extreme reaction temperature, higher reaction time, and high pressure is necessary to the reaction mixture especially when the operating temperature is above the boiling point of the corresponding alcohol in order to maintain the reacting alcohol in liquid state (Issariyakul and Dalai, 2014). The common drawbacks of convectional esterification catalysis mentioned above (homogeneous and heterogeneous catalysis) are the high temperature and pressure requirement that are involved during the esterification. Therefore, there is an urgent need to explore a technology that can efficiently reduce the FFA content of the oil as a pre-treatment step for biodiesel production under ambient conditions.

2.4 Effect of Process Parameters on Esterification Process

2.4.1 Alcohol type and methanol to oil ratio

Esterification can be carried out using short chain alcohols. The main alcohols considered are methanol (Ozbay *et al.,* 2008) and ethanol (Marchetti *et al.,* 2007). However, propanol and butanol have also been investigated, (Zabeti *et al.,* 2009). The type of alcohol used influences type of esters formed, with methanol leading to the formation of fatty acid methyl esters (FAME) and ethanol leading to the formation of fatty acid ethyl esters (FAEE). The main advantages of using ethanol are that it can be derived from renewable sources, it is less toxic and it is less

harmful to the environment (Marchetti *et al.,* 2007; Zabeti *et al.,* 2009). In addition, ethanol is more soluble than methanol, though it is less active for the esterification reaction. Methanol and ethanol were compared for the esterification of lauric acid and it was found that at a temperature of 100^{o}C, ester concentration increased from 20.6 wt% to 39.4 wt% when ethanol was replaced with methanol (Cordeiro *et al.,* 2008). The esterification of palmitic acid was also investigated and a conversion of 75% was possible using methanol compared to a conversion of 1% using ethanol at 60^{o}C (Caetano *et al.,* 2009). Since methanol exhibits higher conversion at lower temperature and less expensive than ethanol, methanol was used as reagent for this work.

Esterification is an equilibrium reaction with one mole of alcohol required to convert one mole of FFAs to one mole of FAME and thus increasing the mole ratio should increase the amount of FAME formed (Yan *et al.,* 2009). There is a large variation in the mole ratios reported for esterification. Feng *et al* (2010) found that the highest conversion could be achieved with a mole ratio of 6:1 with no further increase at higher mole ratios and Chabukswar *et al* (2013) reported that a mole of 4:1 was sufficient. In contrast, Caetano *et al* (2009) showed that conversion can be increased for mole ratio up to 63:1. This leads to a conclusion that an optimum value of alcohol to oil ratio can be different, depending on oil quality.

2.4.2 Temperature

Conversion generally increases with increasing temperature until an optimum value is reached. As the temperature increases further the conversion drops rapidly due to deactivation of the catalyst. Esterification reaction has been investigated using temperature in the range of 50-200^{o}C (Ozbay *et al.,* 2008; Park *et al.,* 2010). The boiling point of methanol and ethanol are 64.7^{o}C and 78^{o}C at standard conditions respectively. A reflux condenser is generally needed for

esterification reaction carried out below the boiling point of the alcohol in order to preclude alcohol loss (Ozbay *et al*., 2008). As the temperature approaches the boiling point of the corresponding alcohols, bubbles are formed and this retards mass transfer and thus reducing conversion (Zabeti *et al.,* 2009). Therefore, a pressure vessel is required to carry out esterification reaction at temperature above the boiling point of alcohol. Cordeiro *et al* (2008) found that increasing the temperature for the esterification of lauric acid from 100^{o}C to 140^{o}C increased the ester content from 39.4 wt% to 87.1 wt%

2.5 Photocatalysis

The word photocatalysis is of Greek origin comprising of two parts: the prefix "photo'' means light and the "catalysis'' means break apart or decompose. Therefore, it can be defined as a chemical reaction induced by photon absorption of a solid material or photocatalyst which remains unchanged during the reaction. A photocatalyst lowers the activation energy of chemical reactions and thus appreciably increases their rate. Chlorophyll of green plants used for photosynthesis can be described as a photocatalyst that captures solar photons and use them to turn water and carbon dioxide into oxygen and glucose while photocatalysis creates strong oxidation agent to breakdown any organic matter to carbon dioxide and water in the presence of photocatalyst, water and light. It can be classified as homogeneous and heterogeneous photocatalysis. Homogeneous photocatalysis, both the reactants and the photocatalyst (semiconductor) are in the same phase. Ozone, transition metal oxide, and photo-fenton systems (Fe^{+} and Fe^{+}/H_2O_2) are most commonly used homogeneous photocatalyst but the main disadvantages of photo-fenton systems are the low pH values which are required, since iron precipitates at higher pH values, high cost of the reagent, and the fact that iron has to be removed. In heterogeneous photocatalysis, both the substrate and the photocatalyst are in

different phases. Most commonly heterogeneous photocatalysts are transition metal oxides and semiconductors. Unlike the metals which have a continuum of electron states, semiconductors possess a void energy region where no energy level is available to promote recombination of an electron and hole produced by photoactivation in the solid. However, more emphasis has been placed on heterogeneous photocatalysis because their non-corrosivity, catalyst reusability, regenerability and environmental friendliness.

2.6 Application of Photocatalysis

Photocatalysis has shown a great potential as a low cost, environmental friendly and sustainable treatment technology to align with the ‘’zero’’ waste scheme in an industry. The ability of this advanced oxidation technology (photocatalysis) has been demonstrated on the use of semiconductor materials as photocatalyst for the elimination of contaminants from water and air, odour control, bacterial inactivation, water splitting to produce hydrogen, the inactivation of cancer cells and many others (Hoffmann *et al*., 1995; Chen *et al*., 2009). However, continuation of extensive research is necessary to further optimize this technology in order to widen the spectrum of potential applications. Few of such applications are discussed in the next sub-sections.

2.6.1 Water treatment

Increasing demand and storage of clean water sources due to the rapid development of industrialization, population growth and long-term droughts have become an issue worldwide. Conventional water treatment methods such as sedimentation, filtration, chemical and membrane technologies involve high operating costs and could generate toxic secondary pollutants into the ecosystem (Gaya and Abdullah, 2008). In view of these downsides, rapid research and

development in the field of "Advanced Oxidation Process (AOPs)'' as a group of innovative water treatment technologies have been explored. Among these AOPs, heterogeneous photocatalysis employing semi-conductor catalysts (TiO_2, Fe_2O_3, ZnO, and ZnS) has demonstrated its efficiency in degrading a wide range of ambiguous refractory organic compounds and water pathogens into readily biodegradable compound, and eventually mineralized them to harmless carbon dioxide and water. Among the semiconductor catalysts, titanium dioxide (TiO_2) has wide application in photocatalytic water treatment due to its chemical and thermal stability or resistance to chemical breakdown and its strong mechanical properties (Chong *et al*., 2010).

2.6.2 Removal of trace metals

Trace metal such as mercury (Hg), chromium (Cr), lead (Pb) and other metals are considered to be highly health hazardous. Thus, removing these toxic metals is essentially important for human health and water quality. The photo reducing ability of photocatalysis has been used to recover expensive metals such as gold (Au), platinum (Pt) and silver (Au) (Bekbolet *et al*., 1998), from industrial effluent.

2.6.3 Destruction of organics

Photocatalysis has been used for the destruction of organic compounds such as alcohols, carboxylic acids, phenolic derivatives, or chlorinated aromatics, into harmless carbon dioxide, water and simple mineral acids. Water contaminated by oil as a result of aging of pipelines, equipment failure, corrosion, accidental operational problem or by sabotage can be treated efficiently by photocatalytic reaction.

2.6.4 Antimicrobial activity

Photocatalysts have been shown to be effective in the disinfection of *Escherichia coli* when combined with other materials. Ferrites combined with silver have been demonstrated to have antimicrobial activity (Li *et al*., 2008). The antimicrobial activity of a photocatalyst is related to its ability to produce hydroxyl radical (OH) on the surface of the catalyst which is highly effective against bacteria. However, the addition of the photocatalyst can greatly increase bacteria disinfection over traditional methods that are used in irradiation with ultraviolet (UV) light alone.

2.6.5 Anti-fogging, self-cleaning of surfaces

Most of the exterior walls of buildings become soiled from automotive exhaust fumes, which contain oily components. When the original building materials are coated with a photocatalyst, a protective film of photocatalyst provides the self-cleaning building in which the hydrocarbon from automotive exhaust is oxidized and the dirt on the walls washes away with rainfall, keeping the building exterior clean.

2.6.6 Reduction of carbon dioxide to methane

Carbon dioxide could be transformed into gaseous hydrocarbon (methane) when it is in contact with water vapour and photocatalyst (titanium oxide) under UV irradiation. Titanium oxide was considered the best choice among several oxides because it has low band gap energy values of approximately 3.0 and 3.2 eV, for rutile and anatase respectively. Illumination by UV light with sufficient photonic energy and appropriate wavelength, generate electrons and holes on the surface of the titanium oxide catalyst, resulting in producing hydroxyl radical and protons. The water will be oxidized by hydroxyl radical producing oxygen and proton and concomitantly, carbon radicals are formed from carbon dioxide through the intermediate product of carbon

monoxide. The carbon radicals then react with protons and electrons on the catalyst surface to finally produce methane (Tan *et al*., 2006).

2.6.7 Destruction of warfare agents

Photocatalysts have the potential of decontaminating chemical warfare agents (CWA) such as, sulfur mustard and the nerve agents that were used in world wars because they contain reactive Lewis acid and basic sites on which adsorption of the CWA and subsequent hydrolysis can take place. Nanoscale metal oxides such as TiO_2, V_2O_5 and clay minerals have shown enhanced reactive properties toward chemical warfare agents due to their high surface, large number of highly reactive edges and corner defect sites (Sharma and Kakkar, 2013).

2.7 Factors Affecting Photocatalyst Activity

2.7.1 Concentration of photocatalyst

The rate of photocatalytic reaction is strongly influenced by the photocatalyst loading, as expected. Heterogeneous photocatalytic reactions are known to show proportional increase in Photodegradation with increasing catalyst loadings (Krysa *et al*., 2004). Generally, in any given photocatalytic application, the optimum catalyst concentration must be determined in order to avoid an ineffective excess catalyst and to ensure total absorption of photons (Saquib *et al*., 2003). This is due to the observation of unfavorable light scattering and reduction of light penetration into the solution with an excess of photocatalyst (Benhebal *et al*., 2013).

2.7.2 Reaction temperature

Experimental evidences for the dependence of photocatalytic activity with temperature have been established by many researchers (Fu *et al*., 1996; Soares *et al*., 2007). Generally, increase in temperature enhances recombination of charge carriers and desorption process of absorbed reactant species, resulting in a decrease of photocatalytic activity. The optimum reaction

temperature for photomineralization has been established to be in the range of 20 - 80^{o}C (Malato *et al.*, 2009).

2.7.3 Nature and concentration of the substrate

Organic molecules which can effectively adsorb to the surface of the photocatalyst will be more prone to direct oxidation (Tariq *et al*., 2007). Thus, the photocatalytic degradation of aromatics depends on the substituent group. Nitrophenol has been reported to be much stronger adsorbing substrate than phenol and therefore degrades faster (Bhakhande *et al*., 2004).

The concentration of organic substrates in time also serves as a determiner for photonic efficiency during photocatalytic oxidation. At high-substrate concentration, however, the photonic efficiency decreases due to an increment of adsorbed compounds and the surface of the semiconductor become saturated, thus leading to catalyst deactivation (Arana *et al*., 2004).

2.7.4 The pH

The pH of the solution is an important parameter in reactions taking place on particulate surfaces as it controls the surface charge properties of the photocatalyst and size of the formed aggregates (Haque and Muneer, 2007). The base line when carrying out photocatalysis is to determine the pH of point zero charge (pH_{pzc}) of the catalyst used. The pH_{pzc} is the pH of the solution in contact with solid at which the net surface charge on the surface of an adsorbent particle is zero. Operating below pHpzc, the surface charge for the catalyst becomes positively charged and gradually exerts an electrostatic attraction force towards the negatively charged compounds while operating above pH_{pzc}, the catalyst surface will be negatively charge and repulsion occurs (Benhebal *et al.*, 2013). Therefore, changes in pH can result in enhancement of the efficiency of photodegradation of organic pollutants.

2.8 Attributes of Good Photocatalysts

The following are the requirements that must be established to certify the suitability of the photocatalyst for use in the industry.

2.8.1 High activity

In general, activity arises from maximizing both the dispersion and availability of the active catalytic material. Ideally, from an activity viewpoint, the catalyst material should be highly dispersed and concentrated on the external surface of the support. Meanwhile, there is an inherent conflict as high concentration of active material becomes progressively more difficult to disperse.

2.8.2 Photo-stability

Photo-instability refers to loss in activity with irradiation time. This deactivation may be caused by aging phenomenon, such as a gradual change in surface crystal surface, by poisoning, which is the irreversible deposition of a substance on the active site. A good photocatalyst should maintain its stability at reaction conditions.

2.8.3 High selectivity and conversion

A good photocatalyst should have a high selectivity at the desired conversion which is usually a high one. This is usually a great problem because higher conversions usually occur at higher temperatures which introduce the problem of catalyst sintering and hence reducing the selectivity of the catalyst and its area of active site available for the reaction. Therefore, to minimize the influence of heat emanating from solar energy, UV lamps, and electrical energy, temperature control is very imperative.

2.8.4 Regenerability

Regenerability refers to the reactivation of a catalyst, which typically will involve air calcination followed in some cases by a re-dispersion of the active component. A good photocatalyst should have the quality that it can be re-generable once deactivation sets in.

2.9 Methods of Improving the Photocatalytic Activity of Semiconductor Photocatalysts

It has been reported that the structural and morphological properties of semiconductors affect its photocatalytic activity (Liao *et al.,* 2008). These properties are the crystalline structure, shape, size, surface area and surface defects. Synthesis methods are the dominant factors affecting the structural and morphological properties of semiconductor photocatalysts. It should be noticed that the photocatalytic activity of a semiconductor is dependent on experimental conditions, properties of the catalyst and the properties of the organic species to be degraded. Many researchers are attempting to improve the photocatalytic activity of semiconductor photocatalysts. Methods for improving the photocatalytic activity of semiconductor photocatalysts include doping technique, dye- sensitizing and semiconductor coupling (Zhu *et al.,* 2010).

2.9.1 Doping technique

Doping is incorporation of atoms or ions in a crystalline lattice i.e., modification of the bulk structure of semiconductor crystallites but not modification of surfaces in order to improve its electrical properties. Band gap of the semiconductor can be altered by doping and excitation of the valence band electrons so the conduction band might be easier due to this induction. Photocatalysts doped with noble and transition metals (e.g., Cu, Co, Ni, Cr, Au, Ag, Pt) have shown improved photocatalytic performance on the degradation of various organic pollutants

(Han *et al.,* 2014; Casbeer *et al.,* 2012). Doping with metals especially metals of large work function such as Au, Pt, and Ag altered the onset of response of semiconductors active under UV (ZnO, TiO_2, ZnS) into visible region.

2.9.2 Dye- sensitization

Organic dyes such as erythrosin B, thionine, methylene blue and phthalo-cyanine are used for surface sensitization of TiO_2 photocatalysts (Korkmaz, 2012). The sensitivity of photocatalysts increase in the visible region and this increase can be explained as the injection of electrons from an excited level of the dye into the conduction band of semiconductor.

2.10 Heterogeneous Photocatalyzed Esterification

Heterogeneous photocatalysis is a novel and cost effective process of reducing FFA content of the oil for biodiesel production. It makes use of abundant visible light present in solar energy; the technology is inexpensive and environmentally friendly. A basic mechanism of photocatalytic esterification proposed by Corro *et al* (2013) is as follows: when heterogeneous photocatalyst (semiconductor) is illuminated by light than its band gap energy, electron-hole pairs diffuse out to the surface of the photocatalyst and participate in the chemical reaction, interacting with surrounding molecules. The free electron and holes transform the surrounding molecules into free radicals (Jang *et al.,* 2006). The surrounding molecules are methanol and FFA present in oil during a heterogeneous photocatalytic esterification of FFA with methanol under irradiation. The photoesterification process can be understood from the schematic energy transfer diagram presented in Figure 2.1

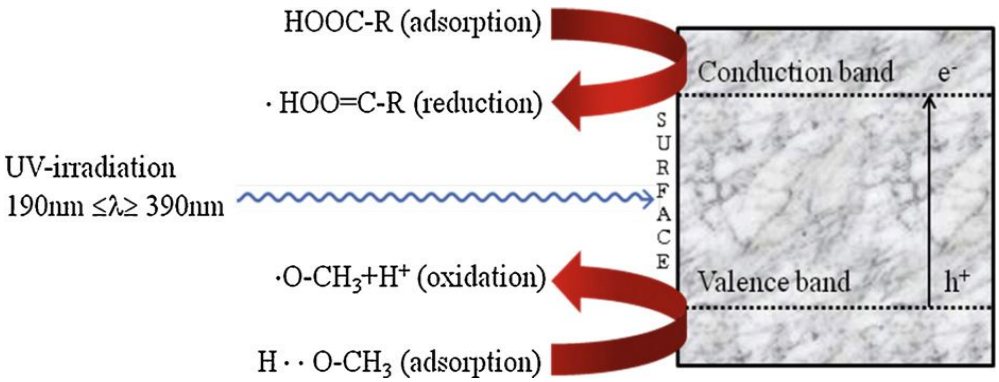

Figure 2.1: Mechanism of Photocatalytic Esterification.

The UV- induced esterification process proceeds in the following steps:

i. Transfer of methanol (CH_3OH) and FFA (HOOC-R) to the surface of photocatalyst. This step may be accelerated by appropriate stirring conditions in the reactor.

ii. Adsorption of methanol and FFA on the photocatalyst surface.

iii. Reaction in the adsorbed phase follows the following steps:

UV photon by composite photocatalyst and generation of photo-induced electron and holes.

Due to high oxidative potential, the photo-generated holes may react with CH_3OH adsorbed on the catalyst surface, producing hydrogen ions (H^+) and CH_3O* radicals in similar way as it has been proposed for the hydrogen production by photocatalytic reforming of methanol (Wu *et al.*, 2008).

$$CH_3O{\cdot\cdot}H + (h^+) \rightarrow CH_3O\cdot + H^+$$

Concomitantly, *HOO=C-R radical might be formed by oxidation of HOOC-R adsorbed at the catalyst surface reacting with photogenerated electron e^- .

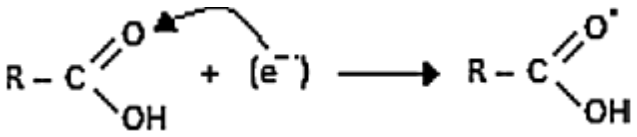

iv. The generated H^+, $^*O\text{-}CH_3$, and *HOO=C-R subsequently would react to form the intermediates and final products.

v. Desorption of the fatty acid methyl ester and water produced during the photoesterification reaction.

vi. Transfer of the products from the interface region to the liquid phase. This step may be accelerated by strong stirring conditions in the reactor.

2.11 Photocatalyst Used in this Work

2.11.1 Zinc oxide (ZnO)

Zinc oxide (ZnO) is one of the most widely employed nano-particles in photocatalytic processes. It is one of the most extensively studied materials because of its outstanding optoelectronic properties, with potential applications in many different fields of technology (Ambrozic *et al*., 2010). Nanopowders controlled to nanocrystalline size (less than 100nm), can show atom-like behaviors, which result from higher surface energy due to their large specific surface area and wider band gap between valence and conduction band when they are divided to near atomic size. Therefore, these phenomena can effectively enhance properties of ZnO including optical, chemical, electro-magnetic, etc. It has been widely used in applications such as photocatalysis, UV protection, thermoelectric materials, functional devices, field emission displays, rubber industry, pharmaceutical and cosmetic industries, and construction industry. Numerous area of its application is attributed to its exceptional physical and chemical properties (Kwon *et al*., 2002).

Ordered and aligned ZnO crystals can be formed into 1- dimensional (1-D) ZnO nanorods, nanoneedles, nanowires by using simple oxidation and chemical processes. Besides that, 2-dimensional (2-D) and 3- dimensional (3-D) ZnO nanostructures can be formed in order to achieve the desire properties required for specific applications. For example, 2-D and 3-D have been explored for bio-chemical sensors as well as light sensing material due to its high specific surface area which could enhance detection and sensing ability.

2.11.2 Catalyst support

A catalyst support is a material, usually a solid with high specific surface area, to which a catalyst is affixed. Catalyst support materials exhibit great influence on the cost, performance and durability of the photocatalyst. One of the most active fields of research in heterogeneous photocatalysis using semiconductor particles is the development of a system capable of utilizing abundant natural sunlight as a sustainable energy source without complicated facilities for generating and introducing UV and visible light to drive photocatalytic process. Some semiconductors are active under UV light. Thus, one of the goals of improving the performance of such semiconductors is to increase their optical activity by shifting the onset of the response from UV to the visible region in order to avoid the high costs of UV lamps and electrical energy. One of the possible approaches to overcome this drawback is by depositing such semiconductors onto the surface of a catalyst support containing some impurities in it. This approach leads to reducing the possibility of electron –hole recombination by increasing the charge separation to increase the efficiency of the photocatalytic process, increasing the wavelength of response range i.e. excitation of wide band-gap semiconductors by visible light and changing the selectivity or yield of a particular product. Other benefits emanate from using catalyst supports in heterogeneous photocatalysis include; precluding breaking down of the photocatalyst in the

reaction mixture, and it can extend life and reusability of the photocatalyst (Fatimah *et al*., 2011). More so, the morphology of the catalyst support, including its porosity, pore volume and internal structure are important criteria for selection of a suitable catalyst support.

2.11.2.1 *Silica (SiO_2)*

The name silica comprises a large class of products with the general formula of SiO_2. Areas of application of silica include the production of glass, ceramics, paint and coating, chemicals, and as proppant to open hydraulic fracture in the reservoir in order to improve the production rate of hydrocarbon.

Mesoporous silica materials with ordered and controllable porous structure, excellent mechanical properties, high specific surface area, pore volume and thermal stability are very suitable catalyst supports for photocatalysis, because they provide high dispersion of metal nanoparticle and facilitate access of the substrates to the active sites (Stein, 2000). The silica used in this work was obtained from Kankara kaolin via dealumination using concentrated sulphuric acid (Salahudeen *et al.,* 2014).

2.12 Supported Photocatalyst

Catalyst support allows more effective utilization of the catalyst than can be achieved in bulk-metal systems. Sometimes, the use of the support is often primarily aimed at improving the catalyst stability. This can be achieved by suitable interaction between the active material and the support. For example: unsupported zinc oxide is a very active oxidation catalyst but suffers from thermal instability at high temperatures. However, when zinc oxide is supported on high-surface-area silica, there is possibility that its thermal stability will be improved (Corro *et al.,* 2013)

Several techniques have been used for incorporation of a catalytically active species onto support materials. Few of such methods are discussed in the next sub-sections.

2.12.1 Impregnation

Impregnation as a route for the preparation of supported catalysts can be accomplished by pervading the pores of a support with a certain amount of solution of the metal precursor for a period of time, dried and calcined. The supported catalyst is synthesized either by spraying the support with the impregnating solution or by adding the support material to the impregnating solution. This method of preparation required in-depth understanding of both the chemical and the physical properties of the support and the chemistry of the solution of metal precursor in order to improve the performance of the catalyst. However, this technique is suitable for the preparation of small amount of catalyst for laboratory studies.

2.12.2 Co-precipitation

Co-precipitation method produces an intimate mixing of solutions containing the metal salt and a salt of a compound that will be converted into the support with the aim of precipitating metal hydroxide or carbonate. By co-precipitation, a uniform distribution on molecular scale of the different active species in the final catalyst could be attained. Nevertheless, many variables have to be controlled during the process. Among the variables are efficient mixing, the procedure and order of addition of the different solutions, the temperature, the ageing time of the precipitate, the filtering and washing procedure and lastly, calcinations temperature. In the preparation of multicomponent catalysts, the pH (value and variation) has to be controlled in order to avoid precipitation of the component at a different sequence, thus affecting the final structure of the solid. This technique is the preferable route for preparing supported catalysts with a metal loading higher than 10-15 % and applicable for production of commercial catalysts (Pinna, 1998).

2.12.3 Chemical vapor deposition (CVD)

Chemical vapor deposition is another technique similar to deposition used in preparing support catalysts. It involves the vapor plating of the support with a volatile inorganic or organometallic compound. The process requires only a moderate vacuum and is currently one of the methods under research in industry as a route of preparing catalysts with a purely surface deposition.

2.13 Preparation of ZnO

Different methods of ZnO synthesis have been intensively reported in the literature including precipitation, spray pyrolysis, hydrothermal synthesis, mechanochemical method, electrochemical method and sol-gel processes (Zhang *et al*., 2009). The ultimate goal the manufacturers are interested in is the ability to control the particle size, particle shape, size distribution, particle composition and degree of particle agglomeration of ZnO. Few processes are discussed in next sub-section.

2.13.1 Hydrothermal method

Hydrothermal synthesis can be defined as a synthesis method for growing single crystals from an aqueous solution at high temperature under high vapor pressure. The technique does not require sophisticated equipment and the crystal can be created directly from the solution, which makes it simple and effective option for large-scale production of ZnO crystals. The size and shape of the obtained ZnO particle is usually controlled by adjusting the reaction temperature, reaction time, reactant concentrations or molar ratio of the precursors used (Djuriscic *et al*., 2012; Yang *et al*., 2009).

2.13.2 Sol-gel method

The sol-gel technique is a long established industrial process for the generation of colloidial nanoparticle by solidification (without precipitation) from liquid phase, which has been further

developed for the production of advanced nanomaterials and coating (Brinker and Scherer, 1990). Sol- gel processes are well adopted for oxide nanoparticles and composites nanopowder synthesis. The general properties of ZnO synthesized by this technique are high purity, high homogeneity, controlled porosity combined with the ability to form large specific surface area at low temperature.

2.13.3 Co- precipitation method

Co-precipitation is a widely used method of obtaining zinc oxide, since the method makes it possible to procure a product with repeatable properties. The method involves fast and spontaneous reduction of a solution of zinc salt using a reducing agent, to preclude the growth of particles with specified dimensions followed by precipitation of ZnO from the solution. The precipitate is then filtered and calcined. However, the process of precipitation is controlled by parameters such as pH, temperature and time of precipitation (Radzimska and Jesionowski, 2014).

2.13.4 Mechanochemical method

Mechanochemical process involves a size reduction and a chemical synthesis that is performed during grinding by which nucleation and growth of the particles can be controlled even in a large scale production. Mechanochemical synthesis involves high-energy dry milling, which initiates a reaction through ball-powder impacts in a ball mill at low temperature. This technique was adopted for current research work due to its simplicity, time saving, and limited propensity for nanoparticles to agglomerate but high energy requirement (Ali *et al*., 2014).

However, there can be difficulties such as agglomeration of the powders, broad particle size distribution and contamination from the process equipment itself. Agglomeration of the powder can be controlled by introducing surfactants, adjusting the milling time and the calcination

temperature (Ao *et al*., 2006). In order to minimize contamination emanating from equipment, less energetic mills are employed. In addition, different factors influencing the milling process have to be considered such as type of mills, milling speed, ball to powder weight ratio, and extent of filling the milling vial, in order to obtain optimum product phase (Ali *et al*., 2014).

2.14 Characterization of Solid Catalysts

Characterization is as important as developing the material, characterization is a judgmental analysis that verifies the type of material that is developed or synthesized. Some conventional characterization techniques are discussed in the next sub-sections.

2.14.1 X-ray diffraction (XRD)

XRD is one of the most important tools used in solid state chemistry and material science. It is a non-destructive technique for qualitative and quantitative analysis of crystalline compounds and for the determination of their structural properties but unable to detect amorphous compounds. A schematic diagram of an XRD is shown in Figure 2.2. X-rays are generated in a sealed tube under vacuum or in a storage ring, when X-ray beam hits the sample the crystal lattice diffracts the x-rays in certain direction in which movable detector scans the diffraction pattern. In normal mode, the detector is set to scan over a 2θ range of 5^0 to 70^0 at a constant angular velocity. The relationship between the angle of diffraction and the distance between the individual lattice planes is described by Bragg's law:

$$n\lambda = 2d\sin\theta \qquad 2.9$$

where λ the wavelength of the incident x-rays, n is an integer number (order of the diffraction peak), θ the scattering angle and d the spacing between the planes in the crystal lattice.

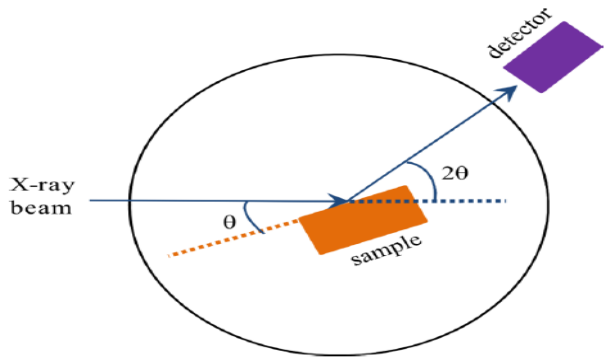

Figure 2.2: A schematic diagram of an XRD.

The (Scherrer's) Equation was developed by Paul Scherrer, to determine the inverse relationship between the width of an x-ray diffraction peak and the crystallite size of the particles in powder form. However, the Equation is limited to nano-scale particles. It is not applicable to grains larger than about 0.1 to 0.2 µm, which precludes those observed in most metallographic and ceramographic microstructures. X-ray diffraction is only sensitive to the crystallite size inside the particle, therefore crystalline size is not the same with particle size.

The mean of crystalline size (D) can be calculated according to Scherrer's Equation which is expressed as

$$D = {0.89\lambda}/{\beta Cos\theta} \qquad 2.10$$

Where, θ is the Bragg angle which can be measured either in radians or degrees, β is the width at half maximum in radians, and λ is the wavelength of x-ray.

2.14.2. Scanning electron microscopy (SEM)

SEM is an instrument that scans a sample surface with a high-energy electron beam in a vacuum chamber. The electron beam comes typically from a tungsten filament and has energy from 0.5 keV to 40 keV. When the electron beam strikes the samples, the electrons interact with the atoms and emit signals that contain information about the sample. The most used signals are the

secondary electrons (SE), the backscattered electrons (BSE) and x-rays. The SE signal comprises vital information on the morphology and topography of the samples. The BSE signal is most valuable for illustrating the contrasts in composition in multiphase samples. The characteristic x-rays are mainly used for elemental analysis. Almost all solid surfaces can be analyzed by SEM. It has a large depth of field, which allows more of a sample to be focused at one time. The SEM also can produce images with high spatial resolution, which means that closely spaced features can be examined at high magnification. All these advantages have made SEM one of the most useful instruments in different research areas today (Suga *et al.*, 2014).

2.14.3 Transmission electron microscopy (TEM)

Transmission electron microscopy (TEM) uses a beam of very energetic electrons. These electrons pass through the sample, whether it is a crystal, a powder, or a biological specimen. The interaction of the electrons with the sample is magnified and detected on a fluorescent screen near the base of the microscope. For an observable amount of electron to pass through the sample, it must be very thin. Consequently, a large amount of time is spent on polishing and thinning the samples compared to the amount of time spent actually viewing the samples in the microscope. TEM can produce images that have higher magnification and greater resolution up to the point where the observer can detect individual atoms than images produced by SEM. This high resolution allows viewing crystals that could not be observed using other methods. In addition to producing high resolution images compared to SEM, another benefit of TEM is that it can switch to diffraction mode to observe the diffraction patterns of different crystal structures. However, the three-dimensional (3D) images produced by SEM provide more information about the shape of features. In some situation, this information is very useful and more important than the higher resolution and magnification that a TEM would provide (Christian, 2014).

2.14.4 X-ray fluorescence (XRF) spectroscopy

XRF is a physical phenomenon involving the interaction of x-ray with matter, which has been used for numerous applications including art verification, biology, biomedicine, pharmaceuticals, electronics, environmental remediation, forensic science, geology and mineralogy, quality control processes and aerospace. The main purpose of using XRF for characterization of materials is to verify the relationship between x-ray energy and atomic number and for quantitative analyses of major and minor elemental compositions. The fundamental principles behind XRF require ionization of component atoms of material when they are exposed to short-wavelength x-rays or gamma rays with energy greater than ionization potential of the materials. X-rays and gamma rays can be energetic enough to expel tightly held electrons from the inner orbits of the atom. The removal of an electron in this way makes the electronic structure of the atom unstable, and electrons in higher orbital fall into the lower orbital to fill the hole left behind. In falling, energy is released in the form of a photon, the energy of which is equal to the energy difference of the two orbitals involved.

However, XRF is limited to analysis of relatively large samples usually greater than one gram, material that can be prepared in powder form and comprising of high abundances of elements for which absorption and fluorescence effects are reasonably well understood (Rollinson, 1993).

2.14.5 Sears' method

This work adopted the empirical method proposed by George W. Sears (1956) for the specific surface area determination of the clay samples by titrating with a base. Detailed procedures and the empirical equation can be obtained in section 3.4.4.4. Sears' method has gained wide application in clay studies (Khraisheh *et al.,* 2004; Bhattacharyya *et al.,* 2009; Tessema *et al.,* 2013; Emeniru *et al.,* 2015). Advantages of using Sears' method are rapidity, accuracy for

particles of very high specific area and applicability to particles in colloidal solution as well as to powders (Sears, 1956). It is worthy of mentioning that the technique gives more accurate result than the nitrogen adsorption method for particles less than 4 to 5μm in diameter. Drying of sample is unnecessary when employing this technique which might caused coalescence of particles and reduction of surface area as in the case of conventional adsorption method where drying is a necessity (Sears, 1956).

2.15 Previous Related Works

It should be noted that preliminary test of photocatalytic activity of the synthesized photocatalysts needed to be investigated on established model compounds (methylene blue and benzoic acid) which have been extensively studied by researchers. Works on photoesterification of biodiesel production are scanty in the scientific literature with only one reported work by Corro *et al* (2013). Therefore, a preliminary study is necessary to ascertain the effectiveness and efficacy of the synthesized photocatalysts as prescribed by International Standard Organization (ISO) of evaluating the activity of photocatalysts.

Ong *et al* (2014) investigated carbon supported copper oxide (CuO/C) catalyst for the esterification of free fatty acids in rubber seed oil. Copper nanoparticles were synthesized by sol-gel method and impregnated into the pore network of the carbon support, calcined at 400^{o}C in a furnace for 6 hours. The effects of reaction temperature, methanol to FFA molar ratio, catalyst concentration on the FFA conversion were also studied. It was revealed from experimental results that methanol to FFA ratio of 10:1, catalyst dose 8wt%, reaction time of 6 hours and temperature of 65^{0}C were found as the optimum (95%) for the esterification reaction.

Wang *et al* (2014) studied the catalytic activity of ferric sulfate (Fs) supported on ordered mesoporous carbon (OMC) for the esterification of the free fatty acids in waste cooking oil with

methanol. The catalyst was synthesized by impregnation method and characterized. The results indicated that the catalyst (Fs/OMC) exhibited excellent catalytic performance for FFA esterification. The highest FFA conversion of 98.4% was obtained using the 10-Fs/OMC catalyst under the optimal esterification reactions: 80^{o}C, 3 wt% catalyst, 30:1 molar ratio of methanol to FFAs and a reaction time of 6 hours. It was reported that the catalyst possessed good activity after six reaction cycles and the amount of iron and sulphur leached from the catalyst into the reaction products was negligible.

Kiwngam and Wanchai (2014) studied the reduction of FFA in waste cooking oil via photocatalytic esterification for biodiesel production using Cu_2O, CuS and Ag_3PO_4 as catalyst under visible irradiation. A conversion of more than 55% was achieved for all the catalysts under the optimal conditions: methanol to oil ratio (21:1) and with irradiation at 200W for 3 hours.

Corro *et al* (2013) esterified the high content of free fatty acids (FFA) present in *jatropha curcas* crude oil (JCCO) with methanol by a photocatalytic process under irradiation using ZnO/SiO_2 as the heterogeneous photocatalyst prepared by impregnation method. The experimental results at a fixed methanol to JCCO molar ratio (12:1) shows that FFA% conversion increased with UV irradiation time and catalyst dose. A conversion of 96% under the optimal conditions of catalyst dose 15 wt% and UV irradiation time of 4 hours was obtained. They also reported that the activity of the catalyst for FFA esterification remains almost unaltered after 10 runs.

Park *et al* (2010) examined the effect of heterogeneous catalyst (WO_3/ZrO_2) on the esterification of free fatty acids from used vegetable oils. The catalyst was prepared by impregnation method and characterized by XRD, BET, and FTIR. Effect of WO_3 loading in the catalyst on the esterification was studied using WO_3 loadings of 10 to 30 wt%. The results revealed that 10

wt%, 20 wt% and 30 wt% of WO_3/ZrO_2 showed FFA conversion of 78%, 93% and 89%, respectively. The effect of the reaction temperature was investigated at a fixed methanol to oil molar ratio of 9:1 and a reaction time of 2 hours from 75 to 200^oC using optimal loading of 20 wt% WO_3/ZrO_2 catalyst. It was concluded that the FFA conversion increased with increasing temperature. At 75^0C, the FFA conversion was 93%, which increased to 98% at 200^oC.

CHAPTER THREE

MATERIALS AND METHODS

3.1 Materials

The main materials used in this work include:

i. Waste Cooking Oil (WCO) obtained from a Restaurant in Samaru, Zaria, Nigeria.

ii. Silica obtained from PTDF Chair Laboratory, Chemical Engineering Department, ABU, Zaria.

iii. Zinc chloride (Analytical grade).

iv. Sodium carbonate (Analytical grade).

v. Sodium chloride (Analytical grade).

vi. Methanol (Analytical grade).

vii. Ethanol (Analytical grade).

viii. Potassium hydroxide pellets (Guarantee reagent) grade.

ix. Phenolphthalein.

x. Isopropanol (Analytical grade).

xi. Benzoic acid (Analytical grade).

xii. Methylene blue (guarantee reagent) grade.

xiii. Distilled water (obtained from Chemical Engineering Department, A.B.U Zaria).

3.2 Apparatus

The apparatus used in this work are:

i. Conical flasks (250, 500ml)

ii. Measuring cylinders (100ml, 1000ml)

iii. Plastic funnels

iv. Retort stand and G-Clamp.

v. Halogen Lamps (500W).

vi. Rubber gloves.

vii. Nose masks.

viii. Spatula.

ix. Crucibles.

x. Filter papers (Wattman).

xi. 100 sample bottles (Plastic).

xii. Syringes (20ml).

xiii. 1 Burette (50ml).

3.3 Equipment

Table 3.1: List of equipment, models/manufacturers, and availability

S/No	EQUIPMENT	MODEL	MANUFACTURE	AVAILABILITY
i	Ball mill machine	Kera BV	Soesterberg, England	Chem.Eng.Lab, A.B.U, Zaria
ii	Digital weighing balance	AV-264 Adventure pro	OHAUS, U.S.A	Chem.Eng.Lab, A.B.U, Zaria
iii	Electric furnace	LH – 120	Naberthaerm GmbH, Germany	Chem.Eng.Lab, A.B.U, Zaria
iv	XRD Machine	Empyreal	PANalytical, England	NGRL,Kaduna
v	XRF Machine	Minipal 4	PANalytical, England	NGRL,Kaduna
vi	GC-MS Machine	QP2010PLUS	Shimadzu, Japan	NARICT,Zaria
vii	SEM Machine	Phenom pro-X	PhenomWorld, Netherland	Chem.Eng.Lab, A.B.U, Zaria
viii	UV-Vis Spectrophotometer	JENWAY- 6405	Edward, England	MultiUser Lab. A.B.U., Zaria
ix	Digital pH meter	JENWAY – 3510	Bibby, UK	Chem.Eng.Lab, A.B.U, Zaria
x	Hot plate with magnetic stirrer	TMOV – 420	Stuart, England	Chem.Eng.Lab, A.B.U, Zaria

3.4 Experimental Procedures (Methodology)

A block diagram of the experimental procedure followed in the course of this work is shown in Figure 3.1

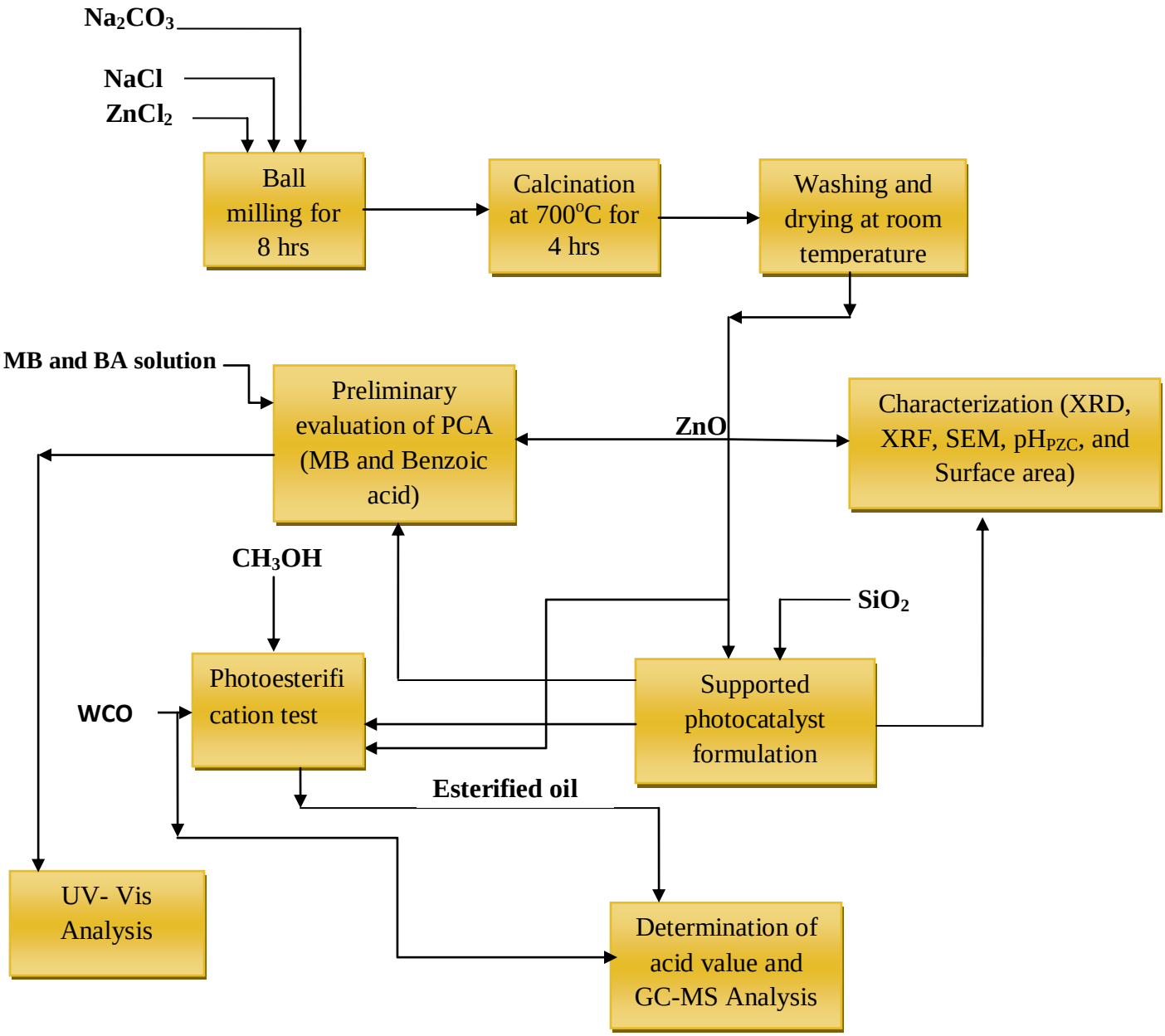

Figure 3.1: Block diagram of the experimental procedure

3.4.1 Synthesis of ZnO

Zinc Oxide (ZnO) was synthesized by mechanochemical method using a high energy ball milling machine (HEBM) according to the procedure reported by Ao *et al*, (2006). The precursors for ZnO, that is, $ZnCl_2$ (50.32g), Na_2CO_3 (39.22g) and NaCl (173.16g) were mixed and milled using a ball milling machine (The molar ratio of NaCl to $ZnCl_2$ was 8:1 and ball to powder weight ratio was 8:1) for 8 hours. Addition of NaCl to the system was used as an inert diluent to prevent agglomeration of the nanoparticles being formed. The reaction of $ZnCl_2$ and Na_2CO_3 proceeds according to the Equation 3.1.

$$ZnCl_{2(s)} + Na_2CO_{3(s)} \rightarrow ZnCO_{3(s)} + 2NaCl_{(s)} \quad 3.1$$

After the milling process, the products obtained from Equation 3.1 were then calcined in an electric furnace (Nabertherm GmbH) at a temperature of 700^oC for 4 hours. ZnO was synthesized according to the calcination step described by Equation 3.2**.** After the calcination, the product was thoroughly washed with de-ionized water and dried at a room temperature for 2 days.

$$ZnCO_{3(s)} \rightarrow ZnO_{(s)} + CO_{2(g)} \quad 3.2$$

3.4.2 Preparation of ZnO/SiO_2

Photocatalyst supports of varying proportion of ZnO/SiO_2 (10 %wt, 20 %wt, 30 %wt, and 40 %wt) were prepared by Solid State Dispersion method (Sharma *et al.*, 2008). The required amounts of ZnO, as shown in Table 3.2, were admixed with silica in absolute ethanol, thoroughly mixed and evaporated (ethanol) at a temperature of 40^0C. After then, the powders of varying proportion of the composites were calcined in an electric furnace at 300^0C for 4 hours.

Table 3.2: Amount of ZnO admixed with SiO_2 for photocatalyst composites preparation

%wt (ZnO/SiO_2)	ZnO (g)	SiO_2 (g)	Sample nomenclature
10	1.0	9.0	10-ZnO/SiO_2
20	2.0	8.0	20-ZnO/SiO_2
30	3.0	7.0	30-ZnO/SiO_2
40	4.0	6.0	40-ZnO/SiO_2

3.4.3 Determination of physico-chemical properties of the waste cooking oil (WCO)

The WCO obtained was filtered to remove particulate impurities and subsequently kept in a tightly covered four- liter plastic container and stored at room temperature to prevent oxidation. A simple titration method (Okpuzor *et al.,* 2009) was used to determine the acid value of the WCO. Each oil sample (1.0g) was weighed and dissolved with 50 ml of ethanol in a conical flask. Two drops of phenolphthalein indicator were added and titrated with 0.1M potassium hydroxide solution until the appearance of the first permanent pink colour which lasted for at least 30 seconds indicating completion of the reaction and the volume of the titre was recorded. The acid values of the initial WCO before and after the photoesterification were determined according to Equation 3.3

$$\text{AV} = \frac{56.1 \text{x} V \text{x} C}{m} \qquad 3.3$$

where V is the volume (ml) of standard volumetric potassium hydroxide (KOH) solution used, C is the concentration (mol/dm^3) of the standard volumetric KOH solution used, m is the mass (g) of the test portion and 56.1 is the molecular mass of KOH.

Saponification value was determined according to titremetric method reported by Pearson (1981). Two grams of oil samples were weighed into a conical flask and 25 ml ethanol potassium hydroxide was added then the solution was refluxed for 30 minutes on a water bath. The mixture was titrated against 0.5 M HCl using phenolphthalein indicator. The same process was conducted for blank determination and the saponification value of WCO was determined according to Equation 3.4

$$\text{SV} = \frac{(B-S)\text{x}28.05}{m} \qquad 3.4$$

where B is the titre value of blank (ml), S is titre value of the sample, and m is the mass of the test portion (2g).

The molecular weight (M) of the oil was determined from the SV and AV according to Equation 3.5 (Cheng *et al.*, 2008)

$$\text{M} = \frac{56.1\text{x}1000\text{x}3}{SV-AV} \qquad 3.5$$

where SV and AV are the saponification and acid values (mg KOH/g), respectively

3.4.4 Characterization of the synthesized ZnO and ZnO/SiO_2 photocatalysts

3.4.4.1 *XRD analysis*

X-Ray Diffraction (XRD) patterns of the synthesized photocatalysts were recorded using a PANalytical England Philips diffractometer at the National Geological Research Laboratory (NGRL), Barnawa, Kaduna with a crystal monochromator at an accelerating voltage of 40kV with 100-mA flux. The X-ray source was CuKα1 with a wavelength of 1.5406Á.

3.4.4.2 *XRF analysis*

Chemical composition of the raw samples was obtained by XRF analysis using a PANalytical England Philips diffractometer at the National Geological Research Laboratory (NGRL), Barnawa Kaduna with a 15kV acceleration voltage and 10 nA beam current.

3.4.4.3 *SEM analysis*

Scanning Electron microscopy (SEM) for microstructures and morphologies of the synthesized photocatalysts were determined using a PHENON PRO-X machine at Chemical Engineering Department, A.B.U Zaria.

3.4.4.4 *Surface area analysis using the Sear's method*

Specific surface area (SSA) of the unsupported ZnO and photocatalyst composites was estimated according to Sear's method (Sears, 1956). A sample of the powdered photocatalyst (0.5g) was acidified with 0.1 mol.dm^{-3} HCl to a pH 3- 3.5. The volume was made up to 50 cm^3 with distilled water after the addition of 10.0 g of NaCl. The solution was titrated with standard 0.1 mol.dm^{-3} NaOH and the volume (V) required to raise the pH from 4.0 to 9.0 was recorded. Then specific surface areas of the synthesized photocatalyst were computed from the Equation 3.6

$$S\ (m^2.g^{-1}) = 32V-25. \qquad 3.6$$

where V, is the volume of NaOH in cm^3 and S, is the specific surface area in m^2g^{-1}.

3.4.4.5 *Determination of point of zero charge (PZC) using the pH drift method*

The point of zero charge (PZC) was determined to find the surface charge of the ZnO and its composites. For the determination of PZC, 0.1 M KCl was prepared and its initial pH was adjusted between 2.0 and 12.0 by adding either NaOH or HCl. Then, 25 mL of prepared 0.1 M KCl was taken in the 100 mL flasks and 50 mg of sample was added to each solution. These flasks were shaken via shaker machine for 1 hour and the final pH was measured and plotted

against the initial pH. The pH at which the plotted curve intersects the line of pH (final) = pH (initial) was taken as the pH_{PZC} of the sample surface.

3.4.5 Photocatalytic degradation of methylene blue and benzoic acid

Methylene blue (MB) and benzoic acid were chosen as model substrates for preliminary photocatalytic activity test. Photocatalytic activity of unsupported ZnO and its composites of varying proportions were evaluated by the degradation of aqueous MB and benzoic acid solutions. 10 mg/L of MB and 20 mg/L of benzoic acid were prepared as stock solutions. 0.1g of unsupported ZnO and its composites (20%, 30%, and 40%) were added to 100 ml of MB and benzoic acid solution (0.1g/100 ml), then stirred for 30 minutes in dark to reach adsorption-desorption equilibrium which was then illuminated under solar light. The solar experiment lasted for 90 minutes. Samples were taken at 15 minutes interval. The analytical samples were filtered, and analyzed for the residual concentration of the pollutants with a JENWAY (6405) UV-Vis spectrophotometer in the Chemistry Department, ABU Zaria. Absorbance data were recorded at the λ_{max} of 665 nm and 225 nm for MB and benzoic acid, respectively. The percentage degradation was calculated using Equation 3.7

$$\text{Degradation}\,(\%) = \frac{A_0 - A_t}{A_0} \text{ X } 100\%. \qquad 3.7$$

where A_0 is the maximum absorbance at time zero (t=0) and A_t is the maximum absorbance on the absorption spectra of the MB and benzoic acid solutions over time (t= 15, 30, 45, 60, 75 and 90 minutes).

As for low concentrations of aqueous MB and benzoic acid solutions, first- order kinetic was used to determine Photodegradation rate constant (K_{app}) of the pollutants using Equation 3.8

$$Ln\, {A_0}/{A} = k_{app}\, t \qquad 3.8$$

where K_{app} is the apparent Photodegradation rate constant and A_0 and A_t are the initial and reaction absorbance of aqueous solution, respectively.

3.4.6 Control experiments on waste cooking oil

3.4.6.1 *Photochemical esterification*

Photochemical esterification experiment of waste cooking oil (WCO) was performed in a 500 ml conical flask in the absence of a photocatalyst. A measured amount of WCO and methanol in a WCO: methanol of 12:1 was placed in the flask. The mixture was stirred with magnetic stirrer and exposed to light of lamp power of 100 W, 200 W, and 500 W. The reaction lasted for an irradiation time of 4 hours. Samples were taken at 1 hour interval and settled. The acid value (A) of the WCO after the photochemical esterification reaction was determined according to Equation 3.3 while the conversion of FFA ($\%C_{FFA}$) was calculated from the acid number ratio using Equation 3.9.

3.4.6.2 *Esterification in the dark*

Esterification of waste cooking was performed in a 500 ml conical flask and conducted in the absence of light irradiation. A measured amount of WCO and methanol in a WCO: methanol ratio of 12:1 was poured in the flask. Two gram of the synthesized supported photocatalysts (10 – 40 ZnO/SiO_2) were added to the mixture and stirred with magnetic stirrer for 6 hours. The obtained reaction mixtures were taken, settled, and filtered. The acid value (A) of the WCO after esterification reaction in the dark was computed from Equation 3.3 while the conversion of FFA ($\%C_{FFA}$) was obtained from the acid number ratio using Equation 3.9.

3.4.7 Photocatalytic esterification of waste cooking oil

Photoesterification experiment of waste cooking oil (WCO) was performed in a 500 ml conical flask. A measured amount of WCO and methanol in a WCO: methanol ratio of 12:1 was placed in the flask. A fixed amount (2g) of a photocatalyst was added to the mixture and stirred with a magnetic stirrer and exposed to light (500 W halogen lamp). The photocatalytic esterification reaction lasted for an irradiation time of 4 hours. Samples were taken at 1 hour interval. The obtained reaction mixtures of 30 ml at various irradiation times were taken, settled, and filtered.

The acid value (A) of the oil after the photoesterification reaction was determined according to Equation 3.3 while the conversion of FFA ($\%C_{FFA}$) was obtained from the acid number ratio using Equation 3.9

$$\%C_{FFA} = \frac{A_i - A_t}{A_i} \text{ x } 100\%. \qquad 3.9$$

where A_i is the initial acid number of WCO and A_t is the final acid number of WCO after the photoesterification reaction over irradiation time (t= 1, 2, 3 and 4 hours).

Also, photocatalytic esterification experiment of waste cooking oil using only SiO_2 was carried out by adhering to abovementioned experimental procedure.

CHAPTER FOUR

RESULTS AND DISCUSSION

4.1 Physico – Chemical Properties of the Experimental Waste Cooking Oil (WCO)

The physico – chemical properties of the WCO are presented in Table 4.1. The acid value of WCO used in this study was found to be 11.22 mgKOH/g, which corresponds to a free fatty acid value of 5.64 %. The WCO has saponification value and molecular weight of 180.29 mgKOH/g oil and 995.45 g/mol, respectively. The difference in the value when compared to what was reported by Aworanti *et al* (2013) in Table 4.1, might be due to variation in the duration the oil was exposed to heat, oxygen and food during cooking (Issariyakul and Dalai, 2014). It has been reported that transesterification would be cost ineffective when homogeneous base catalyst is being employed if FFA content in the oil were above 1% (Freedman *et al.,* 1984). Therefore, it was necessary to perform a pre-treatment process (esterification) on the feedstock prior to biodiesel production. Details on the determination of physico-chemical properties of the WCO can be obtained from Appendix F.

Table 4.1: Physico-chemical properties of the experimental WCO

Parameter	Value	Previous Related Work (Aworanti *et al*., 2013)
Saponification (mgKOH/g)	180.29	182.00
Acid value (mgKOH/g)	11.22	3.20
Free fatty acid (%)	5.64	1.60
Molecular weight (g/mol)	995.45	968.35

4.2 Characterization of the Synthesized ZnO and ZnO/SiO_2 photocatalysts

It is important to note that XRD patterns and SEM analysis of ZnO and the 40-ZnO/SiO_2 supported photocatalyst only were considered in this study because they showed higher photocatalytic activity when compared to other ZnO/SiO_2 supported photocatalysts. XRF of 40-ZnO/SiO_2 supported photocatalyst was also considered.

4.2.1 XRD analysis

Figure 4.1 shows the XRD patterns of the synthesized ZnO. The XRD analysis was employed to determine crystal structure and crystallite size of the synthesized ZnO powder. The XRD pattern was recorded in the 2θ range from 10 to 75^0. The peaks at 2θ = 31.77^0, 34.42^0, 36.24^0, 47.52^0, 56.57^0, 62.84^0, 66.35^0, 67.91^0, 69.08^0, and 74.48^0 are in good agreement with the Powder Diffraction Standard data (JCPDS No. 36-1451), corresponding to the hexagonal wurtzite structure of ZnO.

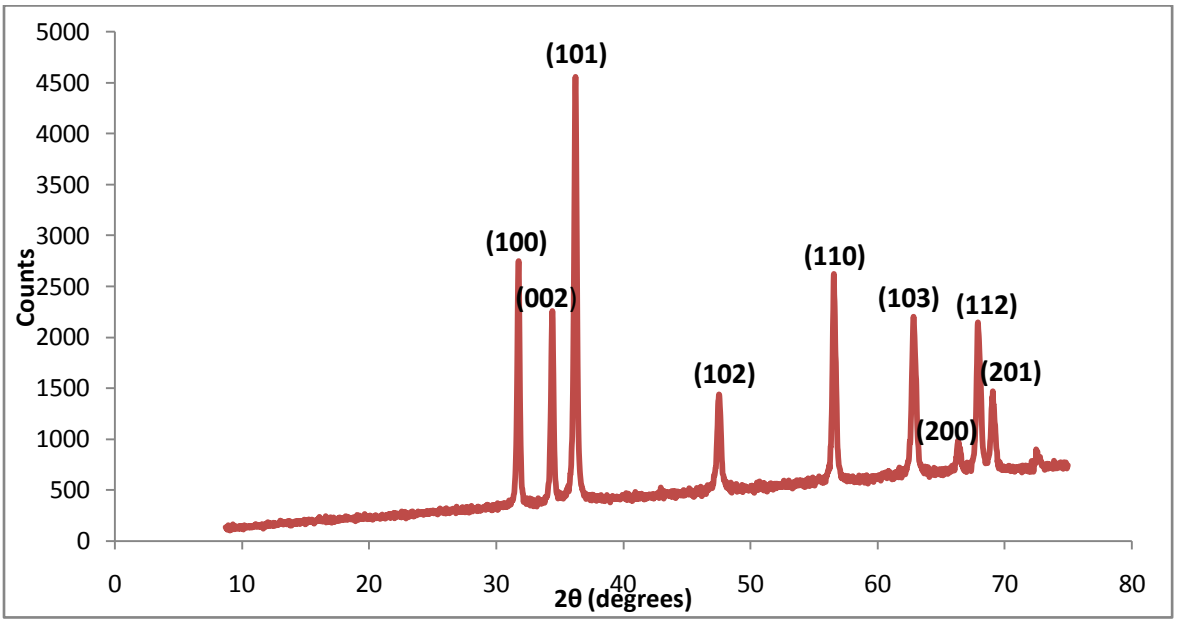

Figure 4.1: XRD patterns of the synthesized ZnO

Since, there was no excess peaks detected apart from peaks of zincite, it showed the complete conversion of $ZnCO_3$ into ZnO at 700 ^{0}C (Aghababazadeh *et al.,* 2006). The strong and sharp diffraction peaks indicated that the synthesized ZnO via this facile mechanochemical method is of high crystalinity.

The crystallite size (D) of the synthesized ZnO was obtained from the full width at half maximum (FWHM) of the peaks using Scherrer's formula. The highest intensity peaks in the XRD patterns (Figure 4.1) was taken as reference peak for computing the crystallite size (D) of the prepared ZnO nanoparticles using Equation 2.10. The computed crystallite size of the synthesized ZnO powder was 34.86 nm, which is similar to the value of 35.00 nm reported by Ao *et al.,* (2006).

Figure 4.2 shows the XRD pattern of the 40- ZnO/SiO_2 composite. A crystalline peak appeared at Bragg's angle of 26.65^0 due to crystalline silica, which also known as quartz (Salahudeen *et al.,* 2014; Ajayi *et al.,* 2010).The quartz peak possessed low intensity. The other peaks observed were rough background peaks due to the presence of silica in amorphous form. The XRD patterns in Figure 4.2 also showed that the characteristic peaks are still in accordance with the wurtzite phase of ZnO, confirming that silica does not have much influence on altering the crystalline structure of ZnO. The same observation had been reported by Siddiquey *et al.,* (2012) and Hong *et al.,* (2009).

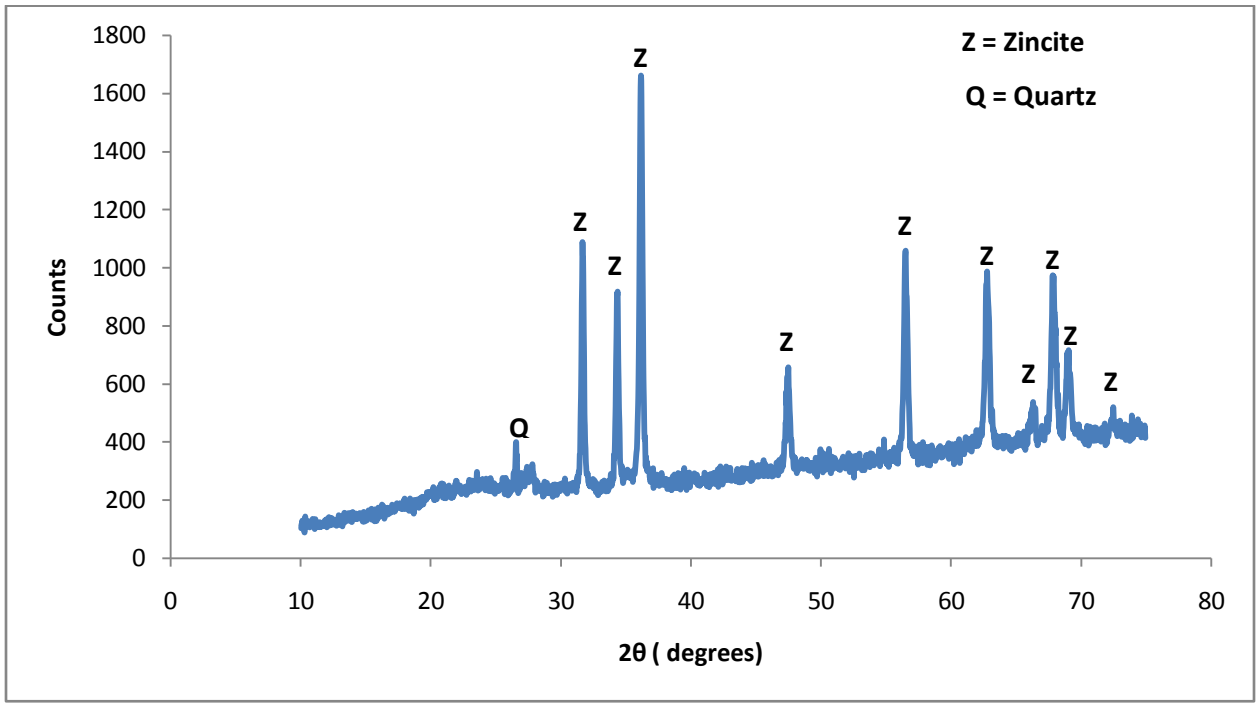

Figure 4.2: XRD patterns of the synthesized 40-ZnO/SiO_2

Also, highest intensity peaks in the XRD patterns (Figure 4.2) was used to compute the crystallite size of the 40- ZnO/SiO_2 supported photocatalysts. The computed crystallite size was found to be 20.92 nm. Although the XRD analysis of other ZnO/SiO_2 supported photocatalysts (10-ZnO/SiO_2, 20-ZnO/SiO_2 and 30-ZnO/SiO_2) were not investigated in line with what was reported by Mohamed *et al* (2013), one can assume that as loading of ZnO on the support increased, there will be appreciable decrease in the intensity peaks of quartz that appeared at Bragg angle of 26.5^0. In other words, the intensity peak of the quartz being crystalline silica will increase corresponding from 40-ZnO/SiO_2 to 10-ZnO/SiO_2.

4.2.2 Scanning electron microscopy (SEM) analysis

Plates 1 and 2 show the scanning electron microscopy (SEM) images of the synthesized ZnO and 40- ZnO/SiO_2 composite, respectively. It can be inferred from Plate 1a that ZnO synthesized via

mechanochemical method composed of tiny particles in submicron range.

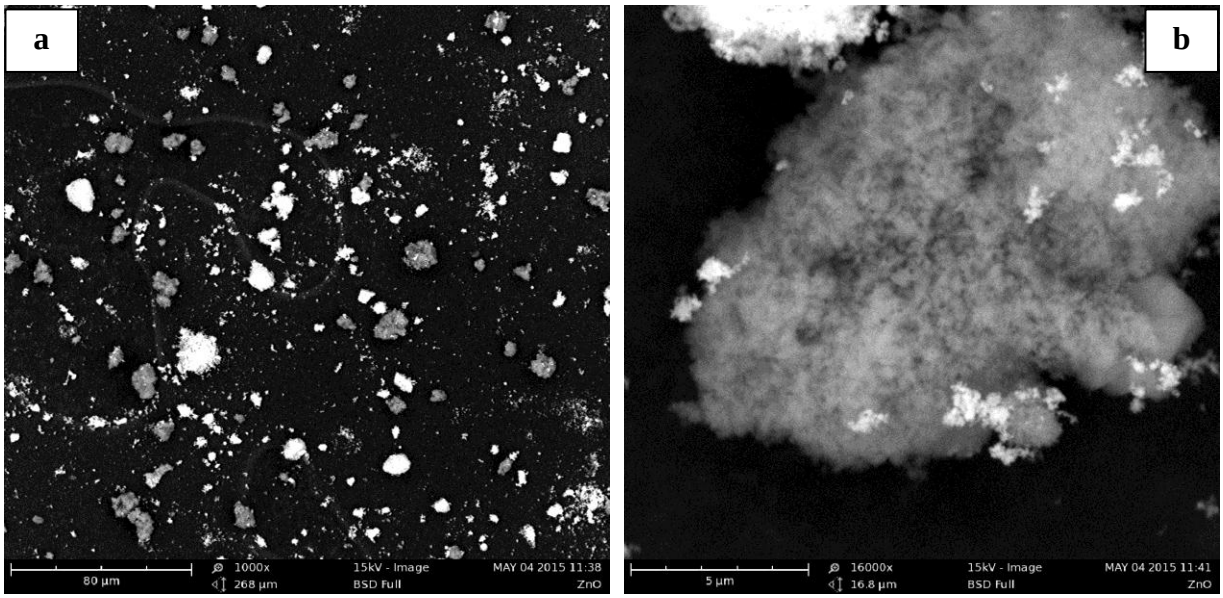

Plate 1: Scanning electron micrographs of the synthesized ZnO (a) at low magnification (1000X) (b) at high magnification (16000X).

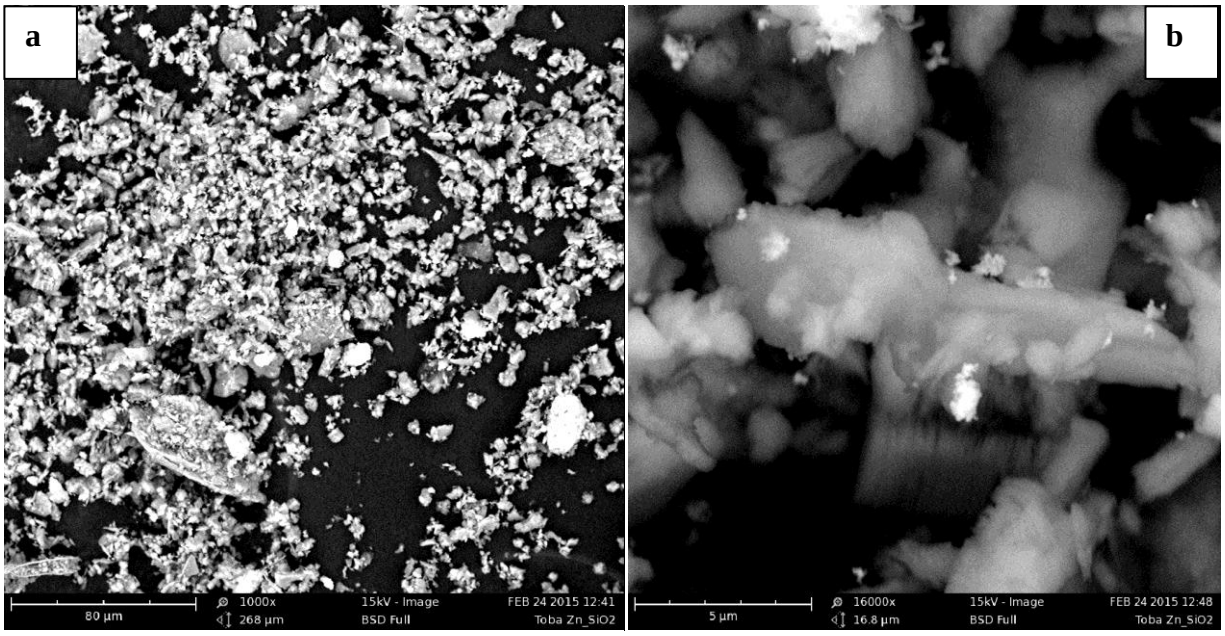

Plate 2: Scanning electron micrographs of synthesized 40-ZnO/SiO_2 composite (a) at low magnification (1000X) (b) at high magnification (16000X)

The surface morphology at higher magnification (Plate 1b) depicts the formation of cluster of particles which was highly homogeneous in nature with less agglomeration due to introduction of surfactant (NaCl) that was used.

At lower magnification (Plate 2a), the particle size is larger than the synthesized ZnO particle (Plate 1a) indicating that SiO_2 when used as catalyst support has much influence on altering the particle size of ZnO. This conforms to the computed particle sizes from XRD results. Also, at higher magnification (Plate 2b) revealed that the composite possessed anhedral sheet-like morphology having irregular structural shapes of silica (Salahudeen *et al.,* 2014). A cursory look at the image in Plate 2b clearly reveals the presence of ZnO deposited on the silica.

4.2.3. Chemical composition of the synthesized 40 - ZnO/SiO_2 supported photocatalyst

Table 4.2 shows the chemical composition of the synthesized 40- ZnO/SiO_2 catalysts. The result indicates that the main constituents are SiO_2 (49.6%) and ZnO (45.22%). Apart from ZnO and SiO_2 that were preponderant, the catalyst also contained lower amounts of other metal oxides (K_2O, CaO, TiO_2, MnO, Fe_2O_3 etc) which all posses some catalytic activity for esterification reaction. Also, absence of alumina (Al_2O_3) component in the synthesized catalyst indicated that the obtained SiO_2 from Kankara kaolin was well separated from alumina via dealumination. Even though 40- ZnO/SiO_2 was synthesized but the XRF showed 45.22%. This might be due to light elements such as sodium, phosphorous, magnesium, lithium, beryllium that could not be detected using XRF but accumulated on ZnO.

Table 4.2: Chemical Composition of the Synthesized 40-ZnO/SiO_2

Component	Concentration wt%	Component	Concentration wt %
SiO_2	**49.6**	**ZnO**	**45.22**
SO_3	0.40	Cr_2O_3	0.019
CaO	0.404	TI_2O	0.87
TiO_2	0.071	Er_2O_3	0.038
V_2O_5	0.0083	Nd_2O_3	0.087
MnO	0.023	BaO	0.100
Fe_2O_3	0.293	Ag_2O	1.98
SeO_2	0.22	CuO	0.017
K_2O	0.601		

4.2.4 Specific surface area

The specific surface area of the synthesized ZnO, ZnO/SiO_2 composites, and silica were determined using Sear's method as discussed in Section 3.4.4.4 and the results are presented in Table 4.3.

Table 4.3: Specific Surface Area of the ZnO, ZnO/SiO_2 Supported Photocatalysts, and SiO_2

Photocatalyst	Specific Surface Area (m^2/g)
ZnO	19.5
SiO_2	723.8
10-ZnO/SiO_2	256.6
20-ZnO/SiO_2	272.3
30-ZnO/SiO_2	397.4
40-ZnO/SiO_2	467.8

Typical values of the specific surface area of ZnO range from 11 to 85m^2/g (Ismail *et al.*, 2012). It can be seen from Table 4.3 that the specific surface area of synthesized ZnO via

mechanochemical method was 19.5 m^2/g, which is close to the value (23.28 m^2/g) reported by Aghababazadeh *et al* (2006). The difference in the values might have resulted from calcination temperature used. Aghababazadeh *et al* (2006) calcined at 400 ^0C while in the present work, 700 ^0C was used. It has been reported in the literature that an increase in the calcination temperature caused an increase in the crystallite size with a corresponding decrease in specific surface area (Moballegh *et al.*, 2007). Therefore, it is expected that specific surface area of synthesized ZnO calcined at 400 ^0C would be greater than the one calcined at 700 ^0C. The specific surface area of SiO_2 obtained from Kankara kaolin was 723.8m^2/g. The shift in the value (604m^2/g) reported by Li *et al* (2014) might be due to environmental factors or source of location of the kaolin and method of preparation of the silica. From Table 4.3, it was observed that the specific surface area of the ZnO/SiO_2 supported photocatalysts were higher than the synthesized ZnO which concord that the use of support enhances the specific surface area of the semiconductor photocatalysts. It was also found that as the ZnO loading increases over the support (SiO_2) from 10-ZnO/SiO_2 to 40- ZnO/SiO_2, the specific surface area of the supported photocatalysts increased from 256.6 m^2/g to 467.8 m^2/g. These results indicated that immobilization of ZnO onto silica have much influence on altering the specific surface area of the silica. Reduction of specific surface area of SiO_2 compared to the ZnO/SiO_2 supported photocatalysts indicating that the pores of SiO_2 are being filled by ZnO.

4.2.5 pH at point of zero charge analysis

The pH at point of zero charge (pH_{PZC}) of synthesized ZnO and the ZnO/SiO_2 supported photocatalysts are presented in Table 4.4. The aim of this analysis was to determine the surface charge of the samples.

Table 4.4: pH at Point of Zero Charge of ZnO and ZnO/SiO_2 composites

Sample	pH at Point of Zero Charge (pH_{PZC})
ZnO	8.8
10-ZnO/SiO_2	NA
20-ZnO/SiO_2	8.2
30-ZnO/SiO_2	7.4
40-ZnO/SiO_2	6.8

The measured pH at point of zero charge of synthesized ZnO via mechanochemical method is 8.8, which is close to the values of 8.6 and 9.3 reported in the literature (Benhebal *et al.,* 2013; Topoglidis *et al*., 2001). The difference in the value might be due to the method of preparation. pH at point of zero charge (pH_{PZC}) determines the pH where the surface charge of the material is zero or neutral. Above this pH_{PZC} (8.8), the ZnO surface is negatively charged due to the formation of O^{2-} on the surface while below 8.8, the surface charge of ZnO particles are positively charged as a result of formation of $Zn^{2+.}$ For the ZnO/SiO_2 supported photocatalysts. It was observed that the values decreased from 20-ZnO/SiO_2 to 40-ZnO/SiO_2 which represent shift towards the pH at point of zero charge of SiO_2. This indicates the attachment of silica on the bare ZnO surface. However, there is no reported literature on the pH_{PZC} of various proportions of the composites but it can be seen from Table 4.4 that silica layer had a great influence on altering the pH_{PZC} of ZnO (Dong *et al.,* 2015).

4.3. Photocatalytic Degradation of Methylene Blue (MB)

Prior to photocatalytic experiments, adsorption studies are carried out on the synthesized ZnO and the ZnO/SiO_2 supported photocatalysts for 30 minutes. This time is considered as necessary to ensure adsorption-desorption equilibrium in order to establish the true initial concentration of MB at the beginning of solar irradiation. Before photodegradation of MB, the adsorption equilibrium is measured and found to be less than 13% for all the catalysts. From the results shown in Figure 4.3, it can be inferred that the percentage degradation of MB for the ZnO and ZnO/SiO_2 composites increased with irradiation time. At irradiation time of 90 minutes, ZnO, 20- ZnO/SiO_2, 30- ZnO/SiO_2, and 40- ZnO/SiO_2 gave percentage MB degradation of 54.56%, 16.02%, 30.89%, and 44.02% respectively. These results imply that more photoexiciation of electron- holes pair on the surface of photocatalysts are being generated under solar light at higher irradiation time which consequently accelerating MB degradation on the catalyst surface. A similar phenomenon was reported by Hong *et al* (2006) that the ZnO nanoparticle exhibited higher photocatalytic degradation than ZnO/SiO_2 composite. Also, Mandel and Natarajan (2015) reported that the photocatalytic degradation of the dye increased with increase in ZnO loading. The observed low photocatalytic degradation of MB at low ZnO loading can be explained by the shielding effect of SiO_2 layer formed on the surface of ZnO nanoparticles. The valence and conduction bands of SiO_2 lie far lower and higher in energy than the corresponding bands of ZnO. Therefore, under solar irradiation at low ZnO loading, SiO_2 layer acts as a barrier to preclude the migration of electrons/holes in ZnO to the surface (Palomares *et al.*, 2003).

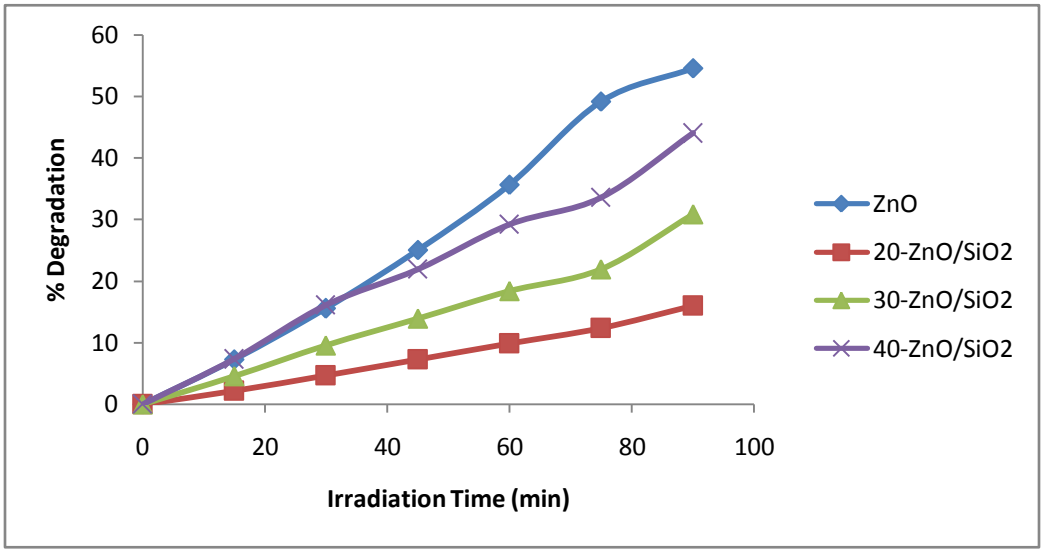

Figure 4.3: Photocatalytic degradation of MB using ZnO and varying proportion of ZnO/SiO_2 supported photocatalysts under solar irradiation

The kinetic parameters of the photocatalytic degradation of MB in aqueous solution with ZnO and ZnO/SiO_2 composites are shown in Figure 4.4, and summarized in Table 4.5. It was observed from Figure 4.4 that the plot of Ln $\frac{C_o}{C_t}$ versus time, gives a fairly good straight line passing through the origin, indicating the photocatalytic degradation of methylene blue follows pseudo first- order kinetics because the correlation constants (R^2) for fitted lines were greater than 0.95 (Figure 4.4 and Table 4.5). The slopes of these lines gave the apparent first order rate constant (K_{app}). The deduced values of K_{app} are 0.008 min^{-1}, 0.001 min^{-1}, 0.003 min^{-1}, and 0.005 min^{-1} for ZnO, 20- ZnO/SiO_2, 30- ZnO/SiO_2, and 40- ZnO/SiO_2 respectively, indicating therefore the order of photocatalytic activity can be ordered as ZnO > 40- ZnO/SiO_2 > 30- ZnO/SiO_2 > 20- ZnO/SiO_2.

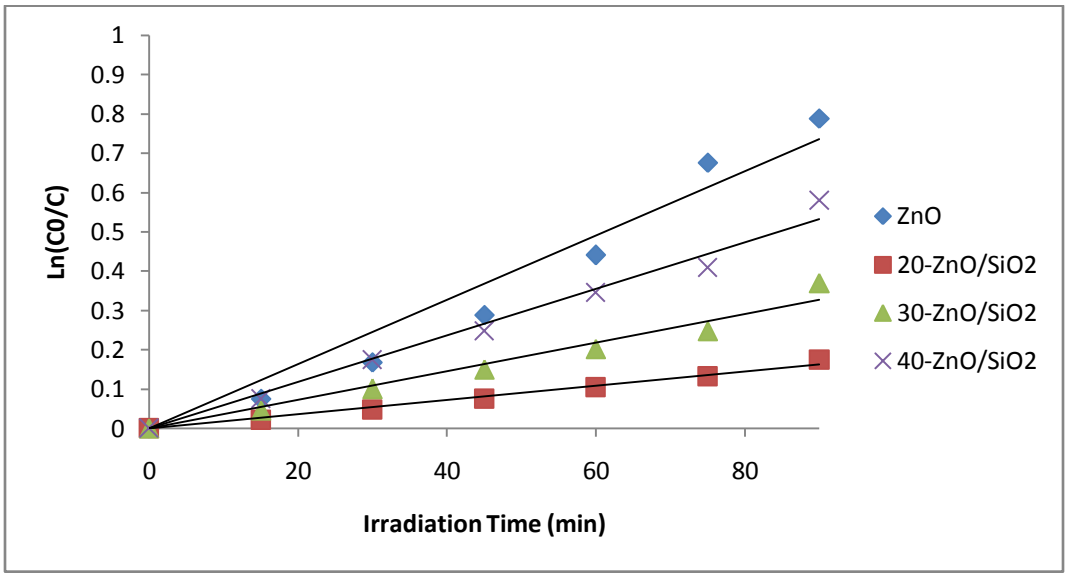

Figure 4.4: Pseudo first order kinetic plot for the solar photocatalytic degradation of MB using the synthesized ZnO and ZnO/SiO_2 supported photocatalysts.

Table 4.5: Values of $K_{app}(min^{-1})$ and R^2 for MB degradation using ZnO and ZnO/SiO_2 supported photocatalysts

Sample	Rate Constant, K_{app} (min^{-1})	R^2
ZnO	0.008	0.956
20- ZnO/SiO_2	0.001	0.987
30- ZnO/SiO_2	0.003	0.969
40- ZnO/SiO_2	0.005	0.983

4.4 Photocatalytic Degradation of Benzoic Acid

The photocatalytic activity of synthesized ZnO and ZnO/SiO_2 supported photocatalysts of various proportions (20- ZnO/SiO_2, 30- ZnO/SiO_2, and 40- ZnO/SiO_2) were also investigated on benzoic acid. Figure 4.5 shows the percentage degradation of benzoic acid as a function of

irradiation time. It should be noted that the trend of the results obtained were similar to the result in Section 4.3.

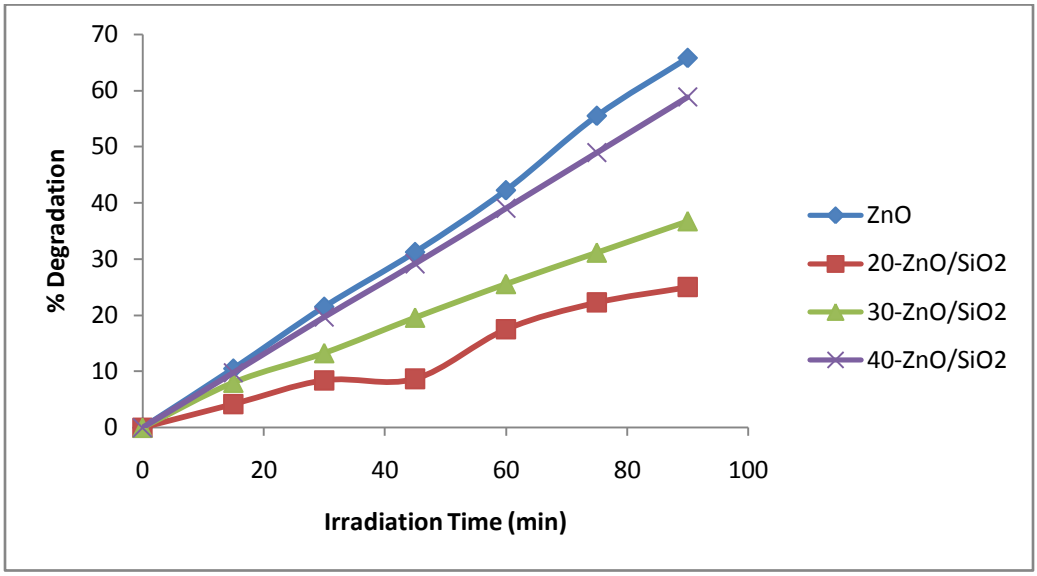

Figure 4.5: Photocatalytic degradation of benzoic acid using ZnO and varying proportion of ZnO/SiO_2 supported photocatalysts as a function of irradiation time

Different ZnO/SiO_2 (weight ratio) supported photocatalysts have varied degradation results. The degradation rate of benzoic acid increased with the irradiation time as shown in Figure 4.5. At irradiation time of 90 minutes, the synthesized ZnO, 20- ZnO/SiO_2, 30- ZnO/SiO_2, and 40- ZnO/SiO_2 supported photocatalysts gave percentage degradation of 65.76%, 25.02%, 36.73%, and 58.80%, respectively. However, experimental studies of ZnO nanoparticle have shown that photocatalytic activity does not increase monotonically with increasing in specific surface area (Liu *et al.*, 2014). The higher photocatalytic degradation exhibited by ZnO though with low specific surface area could be attributed to crystallization, which is another important factor influencing the photocatalytic activity (Yang *et al.*, 2009; Wang *et al.*, 2009). A higher degree of

crystalinity means fewer defects within the lattice and is beneficial for the transfer of photogenerated electron and holes.

The kinetic study of photocatalytic degradation of benzoic acid was also investigated and the results were presented in Figure 4.6 and Table 4.6. Plotting of Ln $\frac{C_o}{C_t}$ against irradiation time in Figure 4.6 gave a linear relation for all the catalysts. This implied that the photocatalytic degradation of benzoic acid can also be described by the pseudo first-order kinetic model. Such kinetics is often observed with photocatalysis (Benhebal *et al.*, 2012; Benhebal *et al.*, 2013). The slopes of the lines which are the apparent rate constants for first order kinetic (k_{app}) and linear regression coefficient (R^2) for synthesized ZnO and the ZnO/SiO_2 supported photocatalysts of various proportions used for the degradation of benzoic acid were listed in Table 4.6. Therefore, ZnO/SiO_2 supported photocatalysts of varying proportions have a significant effect on the degradation rate. The rate constant of degradation of benzoic acid is higher when the loading of ZnO content on silica is increased.

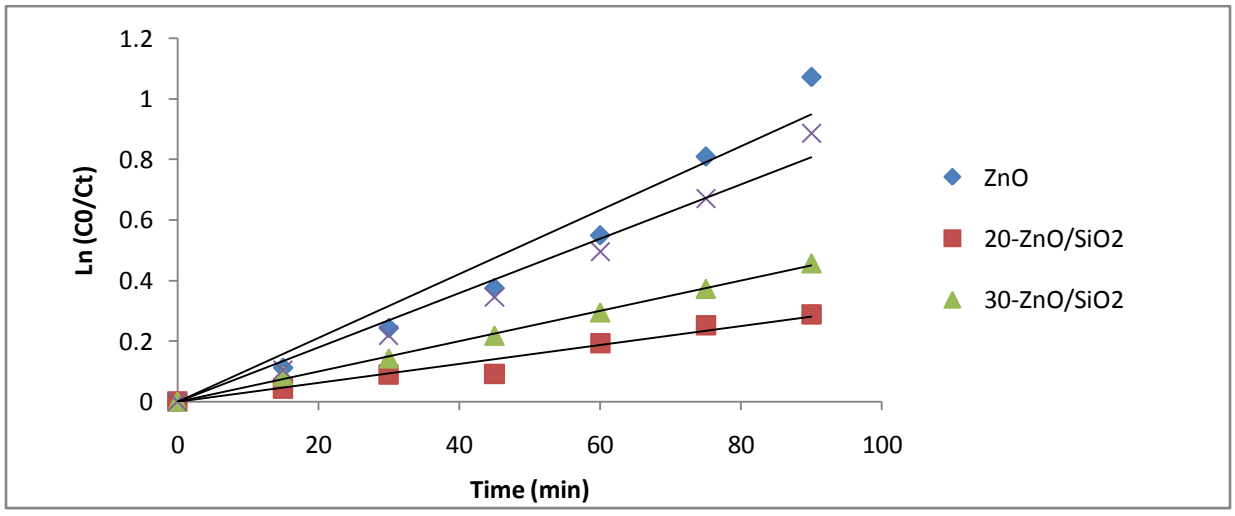

Fig. 4.6: Pseudo first order kinetic plot for the solar photocatalytic degradation of benzoic acid using the synthesized ZnO and ZnO/SiO_2 supported photocatalysts.

Table 4.6: Values of k_{app} (min^{-1}) and R^2 for benzoic acid degradation using ZnO and ZnO/SiO_2 supported photocatalysts

Sample	Rate Constant, $K_{app}(min^{-1})$	R^2
ZnO	0.010	0.954
20-ZnO/SiO_2	0.003	0.959
30- ZnO/SiO_2	0.005	0.998
40- ZnO/SiO_2	0.009	0.974

4.5 Photocatalytic Esterification of Waste Cooking Oil (WCO)

This section presents the results generated using the procedure in Sections 3.4.6 and 3.4.7, together with the corresponding discussions.

4.5.1 Photochemical esterification of waste cooking oil

Figure 4.7 shows FFA conversion as a function of irradiation time. It was observed that the FFA conversion increased with the increase in reaction duration in the absence of a photocatalyst, thus establishing time dependent nature of the reaction. Hwu *et al* (2004) studied photochemical esterification of carboxylic acids with alcohols under UV irradiation and concluded that photochemical esterification proceeds only with the primary and secondary alcohols. The efficiency of photochemical process is often dependent on the intensity of the light photon used.

In this work, light power for the photochemical esterification process was varied between 100W and 500W (as can be seen from Figure 4.7), the %FFA conversion increases with increase in lamp power. These results indicate that reduction of FFA content in WCO could be achieved without a catalyst but strongly depends on the light intensity.

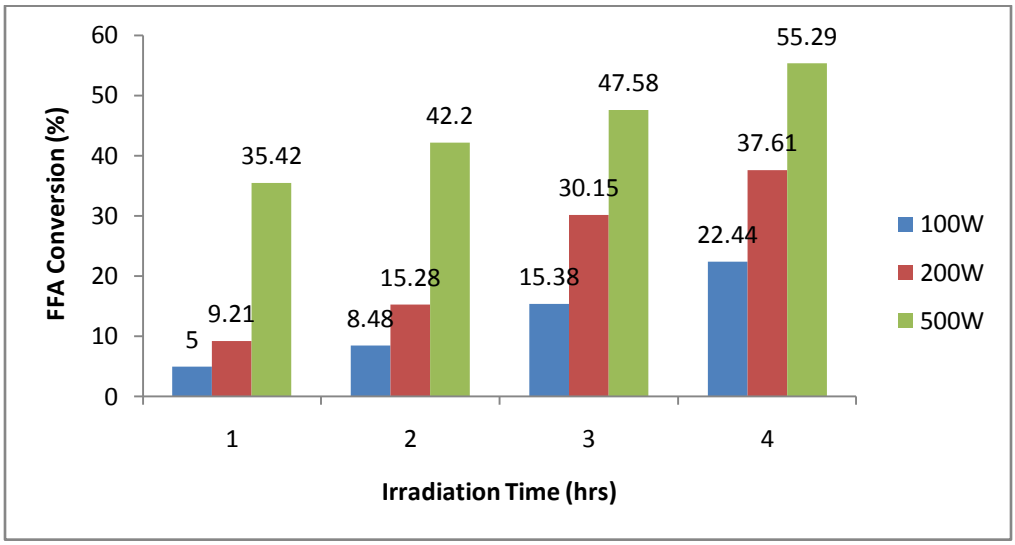

Figure 4.7: Effect of lamp power and irradiation time on photochemical esterification of WCO in the absence of photocatalyst.

4.5.2 Esterification of WCO using ZnO/SiO_2 in the dark

The activity of the synthesized catalysts (10-ZnO/SiO_2, 20-ZnO/SiO_2, 30-ZnO/SiO_2 and 40-ZnO/SiO_2) for the esterification experiments were carried out in the dark and the obtained results are shown in Figure 4.8. It was observed that FFA conversion increases with increase in the ZnO loading. At dark esterification time of 6 hours, 10-ZnO/SiO_2, 20-ZnO/SiO_2, 30-ZnO/SiO_2, and 40-ZnO/SiO_2 exhibited %FFA conversion of 76.4%, 79.9%, 81.5%, and 90.3%, respectively.

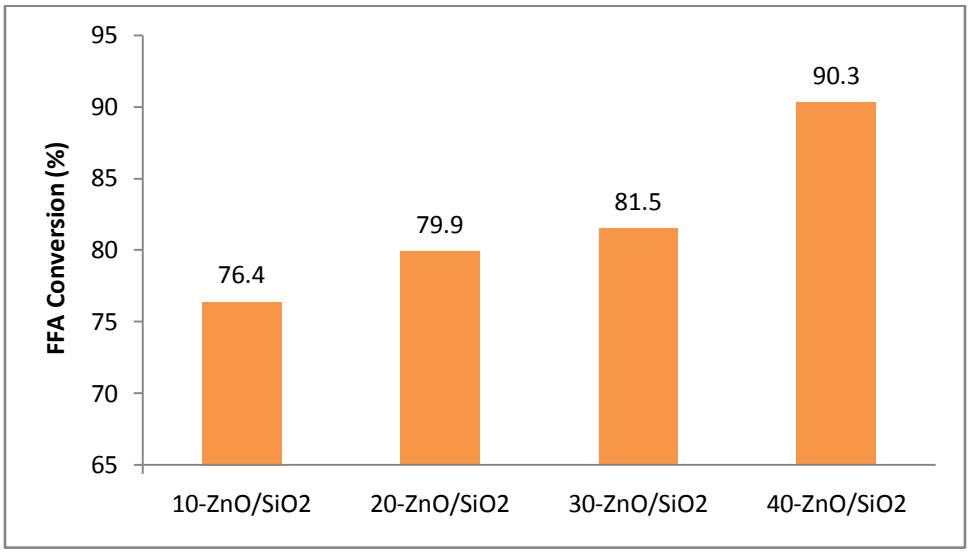

Figure 4.8: Esterification of WCO using the synthesized photocatalysts in the dark (Reaction time: 6hrs, Catalyst dose: 2g)

Considering the fact that ZnO and supported ZnO have been used as excellent catalyst for esterification reaction (Yan *et al*., 2009; Corro *et al*., 2013; Nagvenkar *et al*., 2015), reduction of FFA content in WCO in the dark is possible. Several factors such as acid- base characteristics of ZnO coupled with the presence of base catalysts in the supported photocatalysts (result from Section 4.2.3), the pH of the WCO, and the adsorption capacity measured in term of specific surface area of the synthesized ZnO/SiO_2 supported photocatalysts could be responsible for the observed reduction of FFA in the dark. The higher FFA conversion exhibited by $40\text{-}ZnO/SiO_2$ composite compared to other supported photocatalysts might be correlated with its higher specific surface area as presented in Table 4.3, and high content of ZnO.

4.5.3 Photocatalytic esterification of WCO catalyzed by SiO_2

Control experiment was conducted on the SiO_2 obtained from Kankara kaolin to determine its catalytic activity in the presence of irradiation. The %FFA conversion increased with the irradiation time as presented in Figure 4.9.

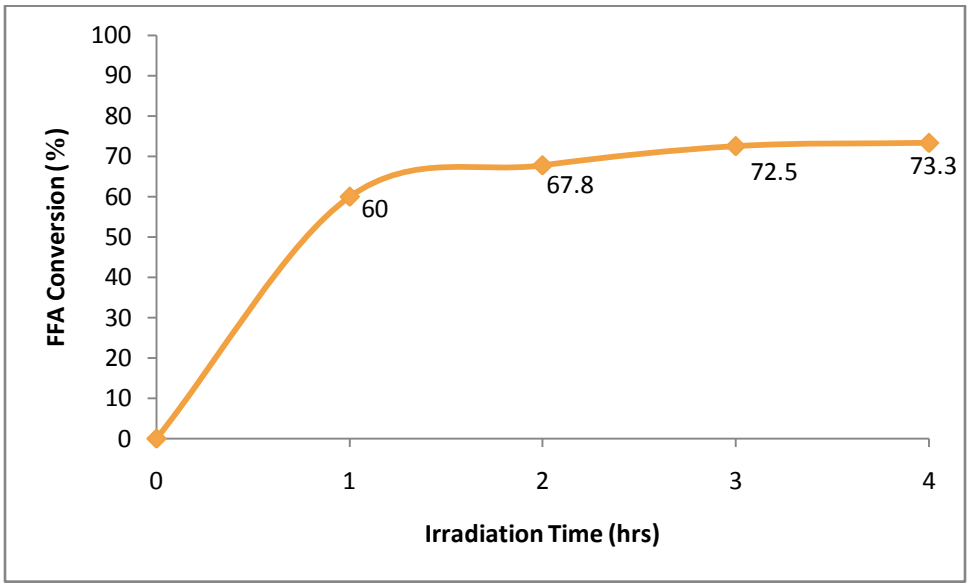

Figure 4.9: Photocatalytic esterification of WCO using SiO_2

From Figure 4.9, it can be seen that SiO_2 is active for FFA photoesterification. Contrary to what was reported by Corro *et al* (2013) that the fused silica was inactive for FFA photocatalytic esterification, the silica used in the present study exhibits some catalytic activity for the photoesterification process. High FFA conversion of 73.3% displayed by SiO_2 was attributed to the presence of basic oxides in the silica which all possess some activity for esterification reaction, combined with cumulative effect of intensity of the light (result from Section 4.5.1), and its high specific surface area (723.8m^2/g) as shown in Table 4.3.

4.5.4 Photocatalytic esterification of WCO using the synthesized ZnO and ZnO/SiO_2 supported photocatalysts

ZnO/SiO_2 photocatalysts were used as heterogeneous photocatalysts for photocatalytic esterification of WCO. As shown in Figure 4.10, FFA conversion increased with increase in ZnO loading as well as reaction time for all the studied ZnO/SiO_2 photocatalysts. At irradiation time of 4 hours, the photocatalyst with higher proportion of ZnO (40-ZnO/SiO_2) exhibits higher FFA

conversion of 94% and that with lower proportion of ZnO (10-ZnO/SiO_2) exhibits lower conversion of 78.6%. This illustrates the role of ZnO loading in the catalytic esterification of WCO. Also, the higher FFA conversion exhibited by 40-ZnO/SiO_2 photocatalyst compared to other photocatalysts could be attributed to its higher specific surface area as presented in Table 4.3. Large specific surface area tends to expose more coordination unsaturated sites on the surface of catalyst and more reactant can be adsorbed onto the catalyst surface for reaction, leading to a higher catalytic activity.

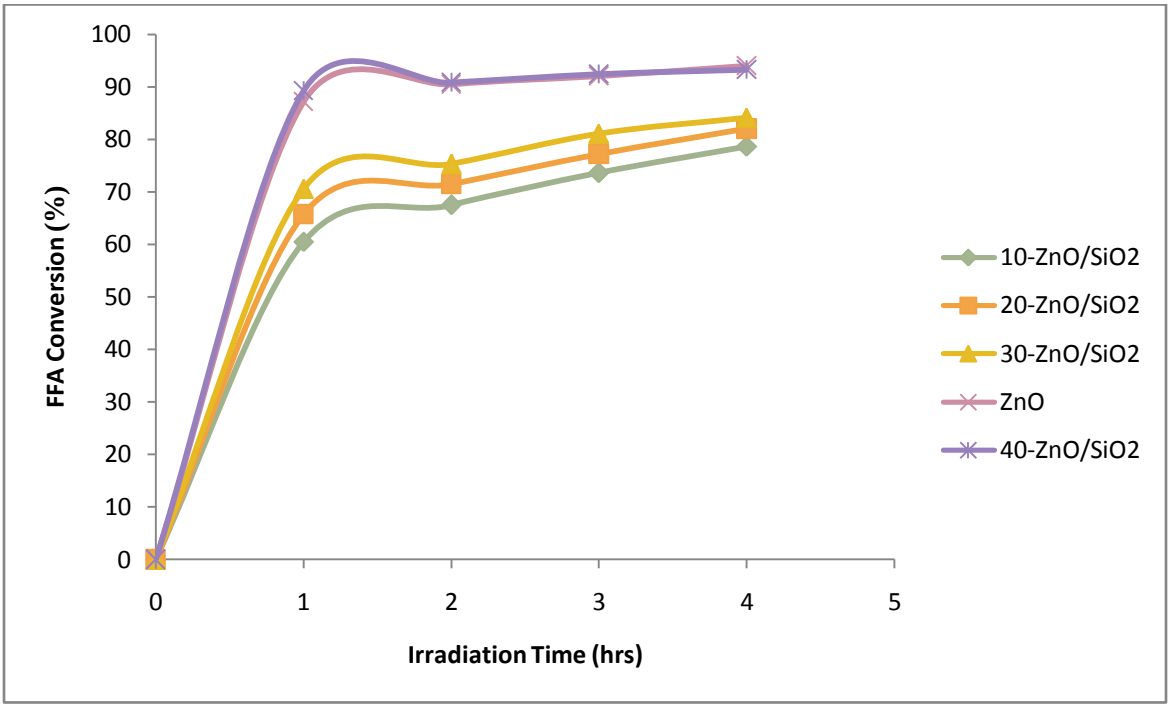

Figure 4.10: Photocatalytic esterification of WCO catalyzed by ZnO and ZnO/SiO_2 composites

ZnO of low specific surface area (19.8m^2/g) gave % FFA conversion of 93.3 when compared to supported photocatalysts with larger specific surface areas. It should be noted that specific surface areas of the catalysts were not solely responsible for the esterification activity (Nagvenkar *et al*., 2015), the cause of enhanced esterification activity of the synthesized ZnO

compared to the ZnO/SiO_2 photocatalysts (10-ZnO/SiO_2, 20-ZnO/SiO_2, and 30-ZnO/SiO_2) could be ascribed to amphoteric nature of ZnO which is another factor responsible for esterification activity (Mitran *et al*., 2015; Nagvenkar *et al*., 2015). These results suggest that more active sites were available on the surface of the synthesized ZnO than the supported photocatalysts (10 to 30- ZnO/SiO_2). FFA could be photo catalytically-esterified using ZnO alone, a technical problem arises with its use due to a strong disaggregation of the ZnO in the reacting mixture. Also, separation of ZnO particles and the liquid phase will be difficult to perform, and a high content of fine ZnO particles will be observed in the final esterified mixture, thus leading to high purification cost for the photocatalytic esterification process (Corro *et al.*, 2013).

4.5.5 GC – MS analysis of the raw and esterified waste cooking oil

The compositions of the waste cooking oil before and after esterification process were identified by comparison of their mass spectra with those of standard mass spectra from National Institute of Standards and Technology Library (NIST 05**)**. The relative peak areas of the components are assumed to be the weight proportion of the components. Table 4.7 shows the compositions of the raw waste cooking oil (WCO). Tables 4.8 and 4.9 present the spectral interpretation for the esterified waste cooking oil in the dark and in the presence of solar energy, respectively. The GC – MS results from Table 4.7, revealed that the main free fatty acids present in the WCO are oleic acid, palmitic acid, Linoleic acid and Stearic acid with oleic acid having a largest % peak area of 56.42 while the least of the acid was Linoleic acid with 5.26% peak area. However, no esters were identified in the raw WCO due to the thermal degradation of the oil during cooking. It is also worthy of mentioning that there are equal number of saturated (palmitic and Stearic) and unsaturated (Linoleic and oleic) fatty acids present in the WCO. But the proportion of the unsaturated fatty acid is higher than that of the saturated fatty acid. Therefore, reduction of

unsaturated fatty acids is imperative due to the fact that heating higher unsaturated fatty acid results in polymerization of glycerides which can lead to the formation of deposits or lead to deterioration of the lubricating ability in the fuel engine (Mittelbach, 1996; Gunstone, 2004). Table 4.7 also presents some harmful compounds or reaction derivatives (Stearyl vinyl ether, Linoleic acid chloride, 4-Ethyl-1-octyn-3-ol, and farnesol) being generated as a result of oxidative, thermolytic, and hydrolytic reaction during oil degradation (Issariyakul and Dalai, 2014), indicating that the WCO should no longer be utilized for edible purpose.

From Table 4.8, it was observed that few methyl esters of low proportion in terms of percentage peak areas were formed during esterification in the dark, and peak areas of oleic and stearic acids increased to 64.10% and 27.04% respectively. It can be assumed that oxidation reaction rather than reduction reaction occurred in the dark leading to an increase in % peak areas of these fatty acids (oleic and stearic acids).

Table 4.9 shows more esters were formed in the presence of light with 13-Methyloxacyclotetradecane-2, 11-dione having the highest predominance as reflected in its percentage peak area of 35.42%. This confirms the conversion of fatty acids being present in Table 4.7 into their respective esters. However, some methyl esters were found in the esterified WCO with no corresponding fatty acids in the raw WCO. This observation could be due to the fact that the corresponding fatty acids were not up to the minimum quantity to be identified in the raw WCO by the GC-MS technique or they were formed during the photocatalytic esterification process.

Table 4.7: GC – MS analysis of the raw waste cooking oil

Retention Time (min)	Compound	% peak area
15.928	Palmitic acid	15.71
17.611	Oleic acid	56.42
17.812	Stearic acid	7.57
18.912	Stearyl vinyl ether	1.28
20.381	Linoleic acid chloride	8.21
22.318	Linoleic acid	5.26
23.013	4-Ethyl-1-octyn-3-ol	3.00
23.627	Farnesol	2.56

Table 4.8: GC – MS analysis of the esterified waste cooking oil in the dark

Retention Time (min)	Compound	% peak area
11.618	Palmitic acid	1.22
15.434	Methyl decanoate	0.99
15.907	Stearic acid	16.15
17.091	Methyl linolelaidate	0.46
17.142	Methyl 11-octadecenoate	1.26
17.615	Oleic acid	64.10
17.792	Stearic acid	10.89
22.293	Brassidic acid	3.36
22.983	6-Methyloctadecane	1.56

Table 4.9: GC – MS analysis of the photocatalytically esterified WCO

Retention Time (min)	Compound	% peak area
10.974	Methyl octanoate	0.64
11.623	Hendecanoic acid	4.39
13.313	Methyl caprate	0.51
13.861	Stearic acid	1.74
15.435	Methyl hexadecanoate	3.97
15.910	Hexadecanoic acid methyl ester	15.91
17.093	Methyl linoleidate	1.94
17.144	Methyl 11-octadecenoate	4.63
17.368	Methyl tridecanoate	0.92
17.608	13- Methyloxacyclotetradecane-2, 11-dione	35.42
17.793	Stearic acid	4.73
21.559	Methyl 2-oxooctadecanoate	8.18
22.290	Tridecanoic acid methyl ester	7.86
22.775	Ocatanoic acid, 2-ethylhexylester	2.93
22.981	Ocatanoic acid, 2-ethylhexylester	4.68

CHAPTER FIVE

CONCLUSIONS AND RECOMMENDATION

5.1 Conclusion

Based on the results obtained in this work, the following conclusions were made:

i. ZnO as well as 10-ZnO/SiO_2, 20-ZnO/SiO_2, 30-ZnO/SiO_2, and 40-ZnO/SiO_2 were synthesized by mechanochemical method followed by solid state dispersion and characterized using XRD, XRF, SEM, pH_{PZC}, and surface area analysis.

ii. XRD result showed that the crystalline structure of ZnO remained unperturbed when supported on SiO_2. However, crystalline peak silica appeared at Bragg's angle of 26.63^0. The specific surface areas of ZnO/SiO2 composites were higher than the specific surface area of the synthesized ZnO ($19.5m^2/g$).

iii. The preliminary photocatalytic evaluation revealed that the photodegradation of methylene blue (MB) and benzoic acid using the synthesized ZnO was 54.56% and 65.76%, respectively, while 40-ZnO/SiO_2 exhibited highest photodegradation of 44.02% for MB and 58.80% for benzoic acid. The activity decreases with decrease in ZnO content of ZnO/SiO_2. The experimental data for the photodegradation of the pollutants (MB and BA) obtained follow pseudo first order kinetic model.

iv. It was observed that the developed catalysts can esterify WCO in the absence of light. However, higher FFA conversion is achieved in the presence of light and the catalysts.

v. Reduction of FFA content in WCO was achieved without a catalyst but the process is less efficient than the photocatalytic esterification and catalytic esterification in the dark.

vi. Based on GC – MS results, there was no occurrence of soap formation and conversion of acids to esters during esterification of WCO was established when ZnO/SiO_2 was used as a photocatalyst for esterification of WCO.

5.2 Recommendation

i. More experiments aimed at understanding the mechanism of photochemical esterification of WCO, catalytic esterification of WCO in the dark using ZnO and ZnO/SiO_2 are highly desired.

ii. The cost benefit(s) of the synthesized photocatalyst should be evaluated.

iii. Process parameters such as molar ratio, catalyst concentration and reaction time affecting esterification reaction should be studied and optimized using design of experiment (DOE).

iv. A pilot plant for esterification process based on solar or visible driven photocatalysis should be developed.

REFERENCES

Aghababazadeh, R., Mazinam, B., Mirhabibi, A. and Tamizifar, M. (2006). ZnO Nanoparticles Synthesized by Mechanochemical Processing. *Journal of Physics : Conference Series,* 26: 312 – 314.

Ajayi, A.O., Atta, A.Y., Aderemi, B.O. and Adefila, S.S. (2010). Novel Method of Metakaolin Dealumination- Preliminary Investigation, *Journal of Applied Sciences Research,* 6(10) : 1539 – 1546.

Ali, M.E., Ullah, M., Maamar, A., Hamid, S.B.A. (2014). Surfactant assisted ball milling: A simple top approach for the synthesis of controlled structure nanoparticle. *Advanced Materials Research*, 832, 356-361.

Ambrozic, G., Skapin, S.D., Zigen, M., Orel, Z.C. (2010). The synthesis of Zinc oxide nanoparticle from zinc acetyacetonate hydrate and 1-butanol or isobutanol. *Journal Colloid Interface Science,* 346, 317-323.

Ameesh, P.M., Vanaja, K.A., Jayaraj, M.K. (2007). In synthesis of ZnO nanoparticles by hydrothermal method, proceeding of SPIE, Gaburro, Z., Cabrini, S. Edition, 66390J.

Ao, W., Li, J., Yang, H., Zeng, X. and Ma, X. (2006). Mechanochemical synthesis of zinc oxide nanocrstalline. *Powder Technology,* 168 : 128-151.

Arana, J., Martinez Nieto, J.L., Herrera Melian, J.A. Dona Rodriguez, J.M., Gonzalez Diaz, O., Perezpena, J., Mendez, J. (2004). Photocatalytic degradation of formaldehyde containing wastewater from veterinarian laboratories. *Chemosphere*, 55, 893-904.

Aworanti, O.A., Agarry, S.E., Ajani, A.O. (2013). Statistical Optimization of Process Variables for Biodiesel Production from Waste Cooking Oil Using Heterogeneous Base Catalyst. *British Biotechnology Journal,* 3(2), 116-132.

Balat, M., Balat, H. (2010). Progress in biodiesel processing. *Applied Energy,* 87, 1815-1835.

Bekbolet, M., Boyacioglu, Z., Ozkaraova, B. (1998). The influence of solution matrix on the photocatalytic removal of colour from natural waters. *Water Science Technology*, 38, 155-162.

Benhebal, H., Chaib, M., Leonard, A., Lambert, D.S. and Crime, M. (2012). Photocatalytic degradation of phenol and benzoic acid by the sol-gel synthesized alkali metal – doped ZnO. *Materials Science in Semiconductor Processing*, 15: 264 – 269.

Benhebal, H., Chaib, M., Salmon, T., Geens, J., Leonard, A., Lambert, D.S. and Heinrichs, B. (2013). Photocatalytic degradation of phenol and benzoic acid using zinc oxide powders prepared by the sol-gel process. *Alexandria Engineering Journal*, 52 : 517-523.

Bhakhande, D.S., Kamble, S.P., Sawant, S.B., Pangarkar, V.G. (2004). Photocatalytic and photochemical degradation of nitrobenzene using artificial ultraviolet light. *Chem. Eng. J.*, 102, 283-290.

Bhattacharyya, K.G., Gupta, S.S. (2009). Adsorptive Accumulation of Cd(II), Co(II), Cu(II), Pb(II), and Ni(II) ions from water onto Kaolinite: Influence of acid activation. *Adsorption Science and Technology*, 27(1), 47 – 68.

Brinker, C.J., Scherer, G.W. (1990). Sol – Gel science: The physics and chemistry of Sol – Gel processing, Academic press, san Diego, CA.

Caetano, C.S., Fonseca, I.M., Ramos, A.M., Vital, J., Castanheiro, J.E. (2008). Esterification of free fatty acids with methanol using heteorpolyacids immobilized on silica. *Catalysis Communication*, 9, 1996-1999.

Caetano, C.S., Zabeti, M., Aroua, M.K. (2009). Esterification of fatty acids to biodiesel over polymers with sulfonic acid groups. *Applied Catalysis A: General*, 359, 41-46.

Carmo Jr, A.C., Desouza, L.K.C., Costa, C.E.F., Longo, E., Zamian, J.R., Rocha Filho, G.N. (2009). Production of biodiesel by esterification of palmitic acid over mesoporous aluminosilicate Al-MCM-41. *Fuel*, 88, 461-468.

Carter, D., Darby, D., Halle, J., Hunt, P. (2005). How to Make Biodiesel, Low – Impacts Living Initiative, *Redfield Community*, Winslow, Bucks, ISSN 0-9649171-0-3.

Casbeer, E., Sharma, V.K., Li, X.Z. (2012). Synthesis and Photocatalytic activity of ferrites under visible light: A review. *Separation and Purification Technology*, 87, 1-14.

Chabukswar, D.D., Heer, P.K.K.S., Gaikar, V.G. (2013). Esterification of palm fatty acid distillate using heterogeneous Sulfonated microcrystalline cellulose catalyst and its comparison with H_2SO_4 catalyzed reaction. *Industrial and Engineering Chemistry Research*, 52, 7316-7326.

Chang, K.H., Chang, D.R., Park, B.G. (2008). Removal of free fatty acid in waste frying oil by esterification with methanol on Zeolite catalysts. *Bioresource Technology*, 99, 7438-7443.

Chen, S., Zaho, W., Liu, W., Zhang, H., Yu, X. (2009). Preparation, characterization and activity evaluation of p-n junction photocatalyst p-$CaFe_2O_4$-ZnO. *Chem. Eng. Journal*, 466-473.

Cheng, J., Li, Y., He, S., Shen, W., Liu, Y., Song, Y. (2008). Reactions kinetics of transesterification between vegetable oil and methanol under supercritical conditions. *Energy Source. Part A*, 30, 681-688.

Chhetri, A.B., Watts, K.C., Islam, M.R. (2008). Waste Cooking Oil as Alternate feedstock for Biodiesel Production, *Energies*, 1, 3-18.

Chong, M.N., Jin, B., Chow, C.W.K., Saint, C. (2010). Recent developments in water treatment technology: A review. *Water Research*, 44, 2997-3027.

Christain, C. (2104). Seeing and measuring with electrons: Transmission electron microscopy today and tomorrow- An introduction. *Comptes Rendus Physique*, 15, 101-109.

Chun, H.Y., Zhong, W., Hongxiao, T. (2002). Destruction of phenol aqueous solution by photocatalysis or direct photolysis. *Chemosphere*, 41, 1205-1209.

Cordeiro, C.S., Miguel, V.U., Lam, M.K. (2008). A new zinc hydroxide nitrate heterogeneous catalyst for the esterification of free fatty acids and the transesterification of vegetable oils. *Catalysis Communications*, 9, 2140-2143.

Corro, G., Pal, U. and Tellez, N. (2013). Biodiesel production from *jatropha curcas* crude oil using ZnO/SiO_2 photocatalyst for free fatty acids esterification. *Applied Catalysis B: Environmental*, 129 : 39 – 47.

Dias, J.M., Alvim-Ferraz, M.C.M., Almeoda, M.F. (2008). Production of biodiesel from acid waste lard. *Journal of Bioresource Technology*, 100(24), 6355.

Djuriscic, A.B., Chen, X.Y., Lung, Y.H. (2012). Recent progress in hydrothermal synthesis of zinc oxide nanomaterials. *Recent Pat. Nanotechnol*. 6, 124-134.

Dong, H., Zeng, G., Tang, L., Changzheng, F., Zhang, C., He, X. and He, Y. (2015). An verview on limitations of TiO_2 – based particles for photocatalytic degradation of organic pollutants and the corresponding countermeasures. *Water Research*, 79 : 128 – 146.

Emeniru, D.C., Onukwuli, O.D., Wodu, P.D., Momohjimo, A.O. (2015). Adsorption characteristics of Ekowe clay and uptake kinetics of methylene blue onto the raw and modified clay. *International Journal of Multididciplinary Sciences and Engineering*, Vol. 6, No. 5

Fatimah, I.S., Wang, S., Wulander, D. (2011). ZnO/Montinorillonite for photocatalytic and photochemical of methylene blue. *Applied Clay Science*, 53, 553-560.

Feng, Y., Ozbay, N., Oktar, N. (2010). Biodiesel production using cation-exchange resin as heterogeneous catalyst. *Bioresource Technology*, 101, 1518-1521.

Fonseca, F.A.S., Vidal-Vieira, J.A., Ravagnani, S.P. (2010). Transesterification of vegetable oil: Simulating the replacement of batch reactors with continuous reactors. *Journal of Bioresource Technology*, 101(21), 8151.

Freedman, B., Butterfield, R.O., Pryde, E.H. (1986). Transesterification kinetics of soyabean oil. *Journal of America Oil Chemists Society.* 63, 1375-1380.

Freedman, B., Pryde, E.H. and Mounts, T.L. (1984). Variables affecting the yields of fatty esters from tranesterified vegetable oils. *J. Am. Oil Chem. Soc*. 61 : 1638 – 1643.

Fu, X., Clark, L.A., Zeitner, W.A., Anderson, M.A. (1996). Effects of reaction temperature and water vapor content on the heterogeneous photocatalytic oxidation of ethylene. *J. Photochem. Photobiol. A*, 97, 181-186.

Gan, S., Ng, H.K., Chan, PH., Leong, FL. (2012). Heterogeneous free fatty acids esterification in waste cooking oil using ion-exchange resins. *Fuel Process Technology*, 102, 67-72.

Gaya, U.I., Abduallah, A.H. (2008). Heterogeneous photocatalytic degradation of organic contaminants over TiO_2: A review of fundamentals, progress and problem. *J. Photochem. Photobiol. C: Photochem.* 9, 1-12.

Gerpen, J.V., Shanks, B., Prusko, R. (2004). Biodiesel Production Technology. Colarado, *National Renewable Energy Laboratory.* Report number. NREL/SR-510-36244.

Gunstone, F.D. (2004). Rapeseed and canola oil: production, processing, properties and uses. London: *Blackwell Publishing* Ltd.

Hameed, B.H., Lai, L.F., Chin, L.H. (2009). Production of biodiesel from palm oil using heterogeneous catalyst: An optimized process. *Fuel Processing Technology*, 90, 606-610.

Han, C., Likodimos, V., Khan, J.A., Nadagouda, M.N., Andersen, J., Falaras, P., Dionysiou, D.D. (2014). UV-visible light activated Ag-decorated, monodisperse TiO_2 aggregates for treatment of the pharmaceutical oxytetracycline. *Environ. Sci. Pollut. Res.* 21, 11781-11793.

Haque, M.M., Muneer, M. (2007). Photodegradation of norfloxacin in aqueous suspension of TiO_2. J. Hazard. Mater. 145, 51-57.

Hara, M. (2009). Environmentally benign production of biodiesel using heterogeneous catalysts. *Sustainable Chemistry, 2,* 671-678.

Hass, M.J., Mcaloon, A.J., Yee, W.C., Foglia, T.A. (2006). A process model to estimate biodiesel production costs. *Bioresources Technology*, 97, 671-678.

Hong, R., Pan, T., Qian, J. and Li, H. (2006). Synthesis and Surface Modification of ZnO Nanoparticles. *Chemical Engineering Journal,* 119 : 71 – 81.

Hong, R.Y., Li, J.H., Chen, L.L., Liu, D.Q., Li, H.Z., Zheng, Y. and Ding, J. (2009). Synthesis, surface modification and photocatalytic property of ZnO nanoparticles. *Powder Technology,* 189 : 426 – 432.

Hwu, J.R., Hsu, C.Y. and Jain, M.L. (2004). Efficient photolytic esterification of carboxylic acids with alcohols in perhalogenated methane. *Tetrahedron Letters,* 45 : 5151 – 5154.

Ismail, B., Stefan, K., Mehtap, S.B. and Martin, M. (2012). Synthesis of High Surface ZnO Powder by Continous Precipitation. *Material Resource Bulletin,* 47(5) : 1185 – 1190.

Issariyakul, T., Dalai, AK. (2014). Biodiesel from vegetable oil. Renewable and *Sustainable Energy Reviews*, 31, 446-471.

Issariyakul, T., Kulkarni, M.G., Dalai, A.K., Bakhshi, N. N. (2006). Production of biodiesel from waste fryer grease using mixed methanol/ethanol system. *Fuel Process Technology*, 88, 429-436.

Jacobson, K., Gopinath, R., Meher, L.C., Dalai, A.K. (2008). Solid acid catalyzed biodiesel production from waste cooking oil. *Applied Catalysis* B, 85, 86-91.

Jang, Y.J., Simar, C., Ohm, T. (2006). *Material Research Bulletin*, 41, 67-73.

Khraisheh, M.A.M., Al – degs, Y.S., Mcminn, W.A.M. (2004). Remediation of wastewater containing heavy metals using raw and modified diatomite. *Chemical Engineering Journal,* 99,177 - 184

Kiwngman, S., Wanchai, K. (2014). Reduction of free fatty acid in waste cooking oil via photocatalytic esterification for biodiesel production. *Burapha University International Conference,* Burapha University, Thailand, July 3-4.

Korkmaz Erdral, B. (2012). Photocatalytic Antimicrobial and self –cleaning properties of Titania-silica mixed oxide thin films' PhD Thesis, Ankara.

Krysa, J., Keppert, M., Jirkersky, J., Stengl, V., Subrt, J. (2004). The treatment effect of thermal treatment on the properties of TiO_2 photocatalyst. *Material Chemical Physics*, 86, 333-339.

Kulkarni, M.G., Dalai, A.K. (2006). Waste Cooking Oil an Economical Source for Biodiesel: A Review. *Ind. Eng. Chem. Res*. 45, 2901-2913.

Kwon, Y.J., Kim, K.H., Lim, C.S., Shim, K.B. (2002). Characterization of ZnO nanopowder synthesized by the polymerized complex method via an organochemical route. *J. Ceram. Process. Res*. 3(3), 146-149.

Lam, M.K., Lee, K.T., Mohammed, A.R. (2010). Homogeneous, heterogeneous and enzymatic catalysis for transesterification of high free fatty acid (waste cooking oil) to biodiesel. A review, *Journal of Biotechnology Advances*, 28(4), 500.

Leung, D.Y.C., Wu, X., Leung, M.K.H. (2010). A review on biodiesel production using catalyzed transesterification. *Journal of Applied Energy,* 87(4), 1083.

Li, S., Lin, Y., Zhang, B., Nan, C., Wang, Y. (2009). Photocatalytic and magnetic behaviours observed in nanostructures $BiFeO_3$ particles. *Journal Applied Physics*, 105, Doi: 056105/1-056105/3.

Liao, D.L., Badour, C.A., Liao, B.Q. (2008). Preparation of nanosized TiO_2/ZnO composite catalyst and its photocatalytic activity for degradation of methyl orange. *Journal of Photochemistry and Photobiology A: Chemistry,* 194.

Liu, K.S. (1994). Preparation of fatty acid methyl ester for gas chromatographic analysis of lipids in biological materials. *Journal American Oil Chem. Soc.* 71(11), 1179-1187.

Liu, R., Wang, X., Zhao, X., Feng, P. (2008). Sulfonated ordered mesoporous carbon for catalytic preparation of biodiesel. *Carbon*, 46, 1664-1669.

Liu, Y., Li, S., Lv, H., Ping, D., Li, S., Li, Z. and Tang, H. (2014). Self – assembly synthesis of ZnO with adjustable morphologies and their photocatalytic performance. *Ceramics International*, 40 : 2973 – 2978.

Lopez, D.E., Goodwin Jr, J.G., Bruce, D.A., Furuta, S. (2008). Esterification and transesterification using modified-zirconia catalysts. *Applied Catalysis A*, 339, 76-83.

Ma, F., Hanna, M.A. (1999). Biodiesel Production: A review. *Bioresource Technology*, 70, 1-15.

Macario, A., Leung, D.Y.C., Lee, K.T. (2010). Biodiesel production process by homogeneous, heterogeneous catalytic system using an acid-base catalyst. *Journal Applied Catalysis A: General*, 378(2), 160.

Malato, S., Fernandez, P., Maldonado, M.I., Blanco, J., Gemjak, W. (2009). Decontamination and disinfection of water by solar photocatalysis: recent overview and trends. *Catalysis Today*, 147, 1 – 59.

Mandal, S. and Natarajan, S. (2015). Adsorption and catalytic degradation of organic dyes in water using $ZnO/Zn_x Fe_{3-x}O_4$ mixed oxides. *Journal of Environmental Chemical Engineering*, 3 : 1185 – 1193.

Marchetti, J.M., Miguel, V.U., Errazu, A.F. (2007). Possible methods for biodiesel production. *Renewable and Sustainable Energy Review*, 11(6), 1300-1311.

Marchetti, J.M., Miguel, V.U., Errazu, A.F. (2007a). Heterogeneous esterification of oil with high amount of free fatty acids. *Journal of Fuel*, 86, 906-910.

Mbaraka, I.K., Shanks, B.H. (2006). Acid strength variation due to spatial location of organosulfonic acid groups on mesoporous silica. *Journal Catalysis*, 244, 78-85.

Mendow, G., Veizaga, N.S., Quermi, C.A. (2011). Ethyl ester production by homogeneous alkaline transesterification: Influence of the catalyst. *Bioresource Technology*, 102, 6385-6391.

Mihai, G.D., Meynen, V., Mertens, M., Bilba, N., Cool, P., Vansant, E.F. (2010). ZnO nanoparticles supported on mesoporous MCM-41 and SBA-15: a comparative physicochemical and photocatalytic study. *Journal Material Science*, 45(21), 5786-5794. doi:10.1007/s10853-010-4652-8.

Mitran, G., Yuzhakova, T., Popescu, I. and Marcu, I.C. (2015). Study of the esterification reaction of acetic acid with n – butanol over supported WO_3 catalyst. *Journal of Molecular Catalysis A: Chemical*, 396 : 275 – 281.

Mittelbach, M. (1996). Diesel fuel derived from vegetable oils, VI: specifications and quality control of biodiesel. *Bioresource Technology*, 56, 7-11.

Moballegh, A., Shahverd, H.R., Aghababazadeh, R. and Mirhabibi, A.R. (2007). ZnO Nanoparticles Obtained by Mechanochemical Technique and Optical Properties. *Surface Science*, 601(13): 2850 – 2854.

Mohamed, R.M., Baeissa, E.S., Mkhalid, I.A., Al-Rayyani, M.A. (2013). Optimization of preparation conditions of $ZnO – SiO_2$ xerogel by sol –gel technique for photodegradation of methylene blue dye. *Applied Nanoscience*, 3: 57 – 63.

Nagvenkar, A., Naik, S. and Fernandes, J. (2015). Zinc oxide as a solid acid catalyst for esterification reaction. *Catalysis Communications*, 65 : 20 – 23.

Ni, Y., Cao, X., Wu, G., Yang, Z., Wei, X. (2007). Preparation, characterization and property study of zinc oxide nanoparticles via a simple solution- combustion method. *Nanotechnology*, 78.

Okpuzor, J., Okochi, V.I., Ogbungafor, H.A., Ogbonnia, S., Fagbayi, T., Obidiegwo, C. (2009). Estimation of cholesterol level in different brands of vegetable oil. *Journal of Nutrition*. 8, 57-62.

Ong, H.R., Khan, M.R., Chowdhury, M.N.K., Yousuf, A., Cheng, C.K. (2014). Synthesis and characterization of CuO/C catalyst for the esterification of free fatty acid in rubber seed oil. *Fuel*, 120, 195-201.

Ozbay, N., Oktar, N., Tapan, N. (2008). Esterification of free fatty acids in waste cooking oil: Role of ion-exchange resins. *Fuel*, 87, 1789-1798.

Palomares, E., Clifford, J.N., Haque, S.A., Lutz, T. and Durrant, J.R. (2003). Control of charge recombination dynamics in dye sensitized solar cells by the use of conformally deposited metal oxide blocking layers. *J. Am. Chem. Soc.* 125 : 475 – 482.

Park, Y.M., Lee, J.Y., Chung, S.H., Park, I.S., Lee, S.Y. (2010). Esterification of used vegetable oils using the heterogeneous WO_3/ZrO_2 catalyst for production of biodiesel. *Bioresource Technology.* 101, 559-561.

Pearson, D. (1981). The chemical analysis of food. Churchill Publishing, London, 580-581.

Pinna, F. (1998). Supported catalysts preparation. *Catalysis Today,* 41, 129-137.

Qiuxiang, Z., Ke, Y., Wei, B., Qiungyan, W., Feng, X., Ziqiang, Z., Yan. S. (2007). Synthesis, optical and field emission properties of three different ZnO nanostructures, *Materials Letters*, 61, 3890.

Radzimska, A.K., Jesionowski, T. (2014). Zinc Oxide – From Synthesis to Application: A Review. *Materials,* 7, 2833-2881

Rollinson, H. (1993). "Using Geochemical Data: Evaluation, Presentation and Interpretation" *John wiley*, NY, 43-47.

Salahudeen, N., Ahmed, A.S., Al- muhtaseb, A.H., Dauda, M., Waziri, S.M. and Jibril, B.Y. (2014). Synthesis and Characterization of Micro – Sized Silica from Kankara Kaolin. *Journal of Engineering Research*, Vol. 19, No 1.

Saquib, M., Munner, M. (2003). TiO_2- mediated photocatalytic degradation of triphenylmethane dye in aqueous suspension. *Dyes Pigments*, 56, 37-49.

Sears, W.G. (1956). Determination of specific area of colloidal silica by titration with sodium hydroxide. *Journal of Analytical Chemistry,* 28(12), 1981 – 1983.

Sharma, N., Kakkar, R. (2013). Recent advancement on warfare agents/ metal oxides surface chemistry and their simulation study. *Advanced Materials Letters,* 4(7), 508-521.

Sharma, M.V., Kumari, V.G., Subrahmanyam, M. (2008). TiO_2 supported over SBA-15: An efficient photocatalyst for the pesticide degradation using solar light. *Chemospere,* 73, 1562 – 1569.

Siddiquey, A.I., Furusawa, T., Sato, M., Bahadur, N.M., Alam, M. and Suzuki, N. (2012). Sonochemical Synthesis, Photocatalytic Activity and Optical Properties of Silica Coated ZnO Nanoparticles, *Ultrasonics Sonochemistry*, 19 : 750 – 755.

Soares, E.T., Lansarin, M.A., Morro, C.C. (2007). A study of process variables for the photocatalytic degradation of rhodamine B. *Brazilian J. Chem. Eng.*, 24, 29-36.

Srilatha, K., Lingaiah, N., Prabhavathi Devi, B.L.A., Prasad, R.B.N., Venkateswar, S., Saiprasad, P.S. (2009). Esterification of free fatty acids for biodiesel production over heterpoly tungstate supported on nobia catalysts. *Applied Catalysis* A, 365, 28-33.

Stein, A., Melde, B.J., Schroden, R.C. (2000). Hybrid inorganic – organic mesoporous silicatenanoscopic reactors coming of age. *Advanced Materials*, 12, 1403-1419.

Suga, M., Asahina, S., Sakuda, Y., Kaznonori, H., Nishiyama, H., Nokuo, T., and Terasaki, O. (2014). Recent progress in scanning electron microscopy for the characterization of fine structural details of nano materials. *Progress on Solid State Chemistry, 42, 1-21.*

Szmigielski, M., Mania, B., Piekarski, W. (2008). Evaluation of chosen quality parameters of used frying rape oil as fuel biocomponent. *International Agro physics,* 22 (4), 361-364.

Tan, S.S., Zou, L., Hu, E. (2006). Photocatalytic reduction of carbon dioxide into gaseous hydrocarbon using TiO_2 pellets. *Catalyst Today,* 15, 269-273.

Tariq, M.A., Faisal, M., Muneer, M., Bahnemann, D. (2007). Photochemical reactions of a few selected pesticide derivatives and other priority organic pollutants in aqueous suspension of TiO_2. *J. Mol. Catal. A.,* 265, 231-236.

Tariq. M., Ali. S., Khalid, N. (2012). Activity of homogeneous and heterogeneous catalyst, spectroscopic and chromatographic characterization of biodiesel: A review. *Renewable and Sustainable Energy Review,* 16, 6303-6316.

Tessema, D.A., Alemayehu, D.D. (2013). A comparative study on Pb^{2+} removal efficiencies of fired clay soils of different particle size distribution. *African Journal of Environment Science and Technology,* Vol. 7(8), 824-832.

Topoglidis, E., Cass, A.E.G., O'Regan, B. and Durrant, J.R. (2001). Immobilization and bioelectrochemistry of proteins on nanoporous TiO_2 and ZnO films. *Journal of Electroanalytical Chemistry,* 517: 20 – 27.

Turkan, A., Kalay, S. (2006). Monitoring lipase – catalyzed methanolysis of sunflower oil by reversed – phase high performance liquid chromatography elucidation of the mechanisms of lipases. *Journal of Chromatography A*, 1127, 34-44.

Wang, L., Dong, X., Jiang, H., Li, G., Zhang, M. (2014). Ordered mesoporous carbon supported ferric sulfate: A novel catalyst for the esterification of free fatty acids in waste cooking oil. *Fuel Processing Technology*, 128, 10-16.

Wang, Y., Du, W. and Xu, Y. (2009). Effect of sintering temperature on the photocatalytic activities and stabilities of hamatite and silica dispersed hamatite particles for organic degradation in aqueous suspension. *Lamgmuir*, 25 : 2895-2899.

Wen, Z., Grisso, R., Arogo, J., Vaughan, D. (2006). Biodiesel fuel, Virgina Cooperative Extension Publication, 442-880.

Wu. G., Chen, T., Su, W., Zhou, G., Zong, X., Lei, Z., Li, C. (2008). Hydrogen production by photocatalytic reforming of methanol. *Journal Of Hydrogen Energy*, 33, 1243-1251.

Xie, W., Huang, X. (2006). Synthesis of biodiesel from soyabean oil using heterogeneous KF/ZnO catalyst. *Catalysis Letters*, 107, 53-59.

Xu. L., W., Hu, J., Yang, X., Guo, Y. (2009). Biodiesel production from soyabean oil catalyzed by multifunctionalized Ta_2O_5/SiO_2-$[H_3PW_{12}O_{40}/R]$ (R=Me or ph) hybrid catalyst. *Applied Catalysis B.* 90(3-4), 587-594.

Yan, S., Salley, S., Simonng, K. (2009). Simultaneous transesterification and esterification of unrefined or waste oil over ZnO – La_2O_3 catalyst. *Applied Catalysis A: General,* 353, 203-212.

Yan, S., Steren, O., Salley, K.Y. and Simon, N. (2009). Simultaneous tranesterification and esterification of unrefined or waste oils over ZnO- La_2O_3 catalyst. *Applied Catalysis A: General,* 353 : 203 – 212.

Yang, J.H., Zheng, J.H., Zhai, H.J., Yang, L.L. (2009). Low temperature hydrothermal growth and optical properties of ZnO nanorods. *Crystal Research and Technology,* 44(1), 87-91.

Zabeti, M., Wan Daud, W.M.A., Aroua, M.K. (2009). Activity of solid catalyst for biodiesel production: A review. *Fuel Processing Technology*, 90, 770-777.

Zhang, Y.L., Yang, Y., Zhao, J.H., Tan, R.Q., Cui, P., Song, W.J. (2009). Preparation of ZnO nanoparticles by a surfactant-assisted complex Sol-gel method using Zinc nitrate. *J.SolGelsci. Technology*, 51,198-203.

Zheng, S., Kates, M., Dube, M.A., Mclean, D.D. (2006). Acid-catalyzed production of biodiesel from waste frying oil. *Biomass Bioenergy*, 30, 267-272.

Zhu, Y.F., Xu, S.B., Y, D. (2010). Photocatalytic degradation of methyl orange using polythiophene/ Titanium dioxide composites, reactive and functional polymers, 70.

APPENDIX A

SYNTHESIS OF ZnO PHOTOCATALYST CALCULATIONS

A calculation for stoichiometric quantity of ZnO synthesized from the precursors ($ZnCl_2$, Na_2CO_3, and $NaCl_2$) is presented in this appendix.

The balance equation is:

$$ZnCl_{2(s)} + Na_2CO_{3(s)} \rightarrow ZnCO_{3(s)} + 2NaCl_{(s)} \quad \text{(A-1)}$$

$$ZnCO_{3(s)} \rightarrow ZnO_{(s)} + CO_{2(g)} \quad \text{(A-2)}$$

Molar mass (g/mol) of each element are:

Zn=65, Cl=35.5, O=16, Na=23, C=12

Basis: 30g of **ZnO**

Material balance over reaction A-2

To produce 30g of Zinc oxide (ZnO)

Molar mass of ZnO = 81g/mol

Mole of ZnO= 30/81 = 0.37mol

Hence, 0.37mol of ZnO is needed.

The amount of $ZnCO_3$ required to produce 30g of ZnO is calculated below;

Molar mass of $ZnCO_3$ = 125g/mol

Mass of $ZnCO_3$ required = 125*0.37 =46.25g.

Hence, 46.25g of $ZnCO_3$ is needed to produce 30g of ZnO.

Material balance over reaction A-1

The amount of $Zncl_2$ required to produce 30g of ZnO is calculated below;

Molar mass of $ZnCl_2$ = 136g/mol

Mass of $Zncl_2$ needed = 0.37*136= 50.32g

Hence, 50.32g of $ZnCl_2$ is required to produce 30g of ZnO.

The amount of Na_2CO_3 required to produce 30g of ZnO is calculated below;

Molar mass of Na_2CO_3 = 106g/mol

Mass of Na_2CO_3 needed = 0.37*106= 39.22g

Hence, 39.22g of Na_2CO_3 is required to produce 30g of ZnO.

The amount of sodium chloride (NaCl) required to be added to the powder as a surfactant/diluent is shown below; N.B: molar ratio of NaCl to $ZnCl_2$ was 8:1

Molar mass of NaCl= 58.5g/mol.

Mass of NaCl= 8*0.37*58.5=173.16g.

Hence, 173.16g of NaCl is required to be added to the powder.

In summary,

To produce 30g of ZnO, we need amount of the following reagents based on the equations illustrated above (A-1, A-2)

$ZnCl_2$ = 50.32g

Na_2CO_3 = 39.22g

NaCl = 173.16g

APPENDIX B

CRYSTALLINE SIZE DETERMINATION FROM XRD DATA

The crystal sizes were determined using Scherer's equation, $D = \frac{K\lambda}{\beta cos\theta}$ from data obtained from XRD analysis. For the samples under discussion, K=0.89, λ=0.1540 nm and $\beta = (\Theta_2 - \Theta_1)\frac{\pi}{180}$

Where, D = particle size, nm

λ=1.54Å

β= width at Full Width at Half Maximum (FWHM) in radians

2θ=Bragg angle

1. The synthesized ZnO;

   At $2\Theta = 36.24^o$, $\Theta_1 = 36.14^o$, $\Theta_2 = 36.38^o$

   $\beta = (36.38 - 36.14)\frac{\pi}{180} = 0.004189$

   $D = \frac{K\lambda}{\beta cos\theta} = \frac{0.9x0.1542}{0.004189xcos\ 18.12} = 34.86nm$

2. 40-ZnO/SiO_2

   At $2\Theta = 36.17^o$, $\Theta_1 = 36.04^o$, $\Theta_2 = 36.44^o$

   $\beta = (36.44 - 36.17)\frac{\pi}{180} = 0.00698$

   $D = \frac{K\lambda}{\beta cos\theta} = \frac{0.9x0.1542}{0.00698xcos\ 18.09} = 20.92nm$

APPENDIX C

SURFACE AREA DETERMINATION USING SEAR'S METHOD

The specific surface areas (SSA) of the samples were determined using Sear's method according to the equation S (m^2/g) = 32V-25

1. ZnO

   Titre values: V_1= 1.41cm^3, V_2=1.37cm^3

   SSA_1= 32x1.41 – 25

   SSA_1= 20.12m^2/g

   SSA_2 = 32x1.37 – 25

   SSA_2 = 18.84m^2/g

   $SSA_{ZnO} = \frac{20.12+18.84}{2}$ =19.48m^2/g

2. SiO_2

   Titre values: V_1= 23.3cm^3, V_2=23.5cm^3

   SSA_1= 32x23.3 – 25

   SSA_1= 720.6m^2/g

   SSA_2 = 32x23.5 – 25

   SSA_2 = 727m^2/g

   $SSA_{SiO2} = \frac{720.6+727}{2}$ =723.8m^2/g

3. 10-ZnO/SiO_2 (10)

   Titre values: V_1= 8.6cm^3, V_2=9.0cm^3

   SSA_1= 32x8.6 – 25

   SSA_1= 250.2m^2/g

   SSA_2 = 32x9.0 – 25

$SSA_2 = 263m^2/g$

$SSA_{10}\ \frac{250.2\ +263}{2} = 256.6m^2/g$

4. 20-ZnO/SiO_2 (20)

   Titre values: V_1= 9.1cm^3, V_2=9.5cm^3

   SSA_1= 32x9.1 – 25

   SSA_1= 266.2m^2/g

   SSA_2 = 32x9.5 – 25

   SSA_2 = 279m^2/g

   $SSA_{20}= \frac{266.2\ +279}{2}$ =272.6m^2/g

5. 30-ZnO/SiO_2 (30)

   Titre values: V_1= 13cm^3, V_2=13.4cm^3

   SSA_1= 32x13 – 25

   SSA_1= 391m^2/g

   SSA_2 = 32x13.4 – 25

   SSA_2 = 403.8m^2/g

   $SSA_{30}= \frac{391\ +403.8}{2}$ =397.4m^2/g

6. 40-ZnO/SiO_2(40)

   Titre values: V_1= 15.2cm^3, V_2=15.6cm^3

   SSA_1= 32x15.2 – 25

   SSA_1= 461.4m^2/g

   SSA_2 = 32x15.6 – 25

   SSA_2 = 474.2m^2/g

   $SSA_{40}= \frac{461.4+474.2}{2}$ =467.8m^2/g

APPENDIX D

DETERMINATION OF pH AT POINT OF ZERO CHARGE USING DRIFT METHOD

Table D: pH values ($pH_{Initial}$ and pH_{Final}) for the photocatalysts

	ZnO	20-ZnO/SiO_2	30-ZnO/SiO_2	40-ZnO/SiO_2
$pH_{Initial}$	pH_{Final}	pH_{Final}	pH_{Final}	pH_{Final}
2	6.52	6.17	2.44	5.10
3	6.74	7.04	6.65	6.72
4	6.82	8.78	7.59	7.00
5	7.06	7.26	7.24	6.94
6	7.55	7.30	7.37	6.23
7	7.77	8.02	7.83	6.38
8	8.58	8.76	7.23	6.72
9	9.02	7.70	7.97	7.47
10	8.15	8.27	8.34	8.09
11	9.31	9.94	9.37	9.20
12	11.76	11.91	11.39	11.00

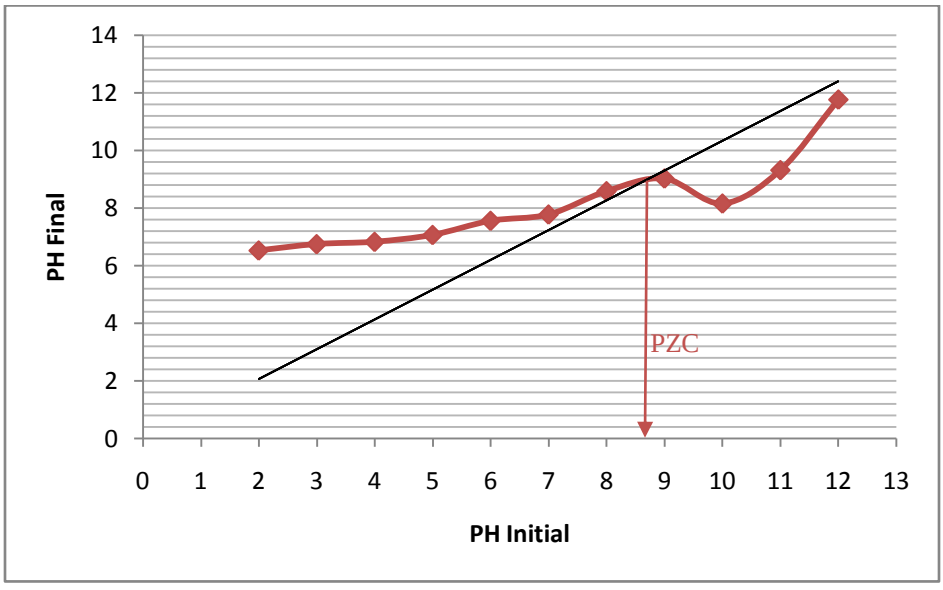

Figure D-1. A plot of pH_{Final} against $pH_{Initial}$ for the synthesized ZnO

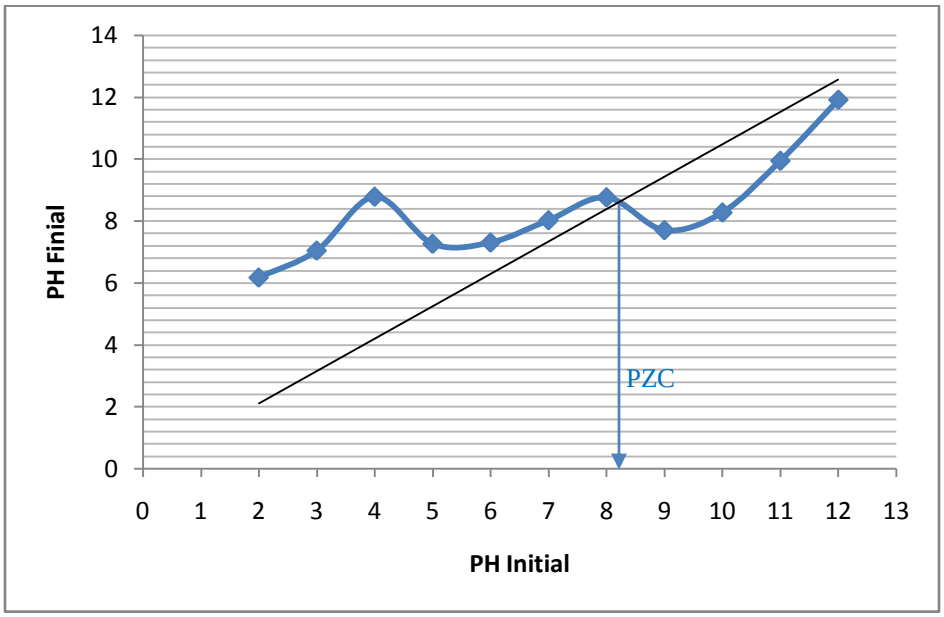

Figure D-2. A plot of pH_{Final} against $pH_{Initial}$ for the synthesized 20-ZnO/SiO_2 photocatalyst

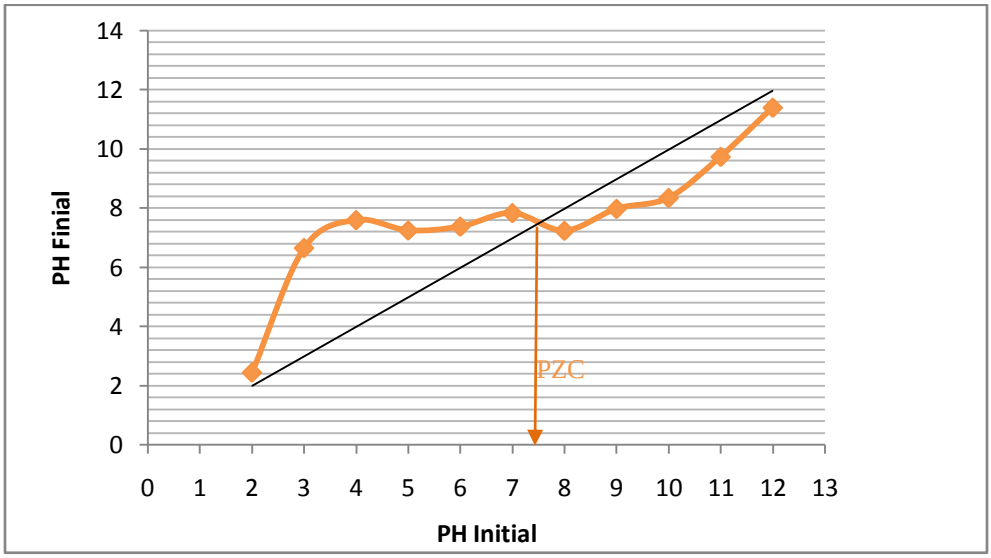

Figure D-3. A plot of pH_{Final} against $pH_{Initial}$ for the synthesized 30-ZnO/SiO_2 photocatalyst

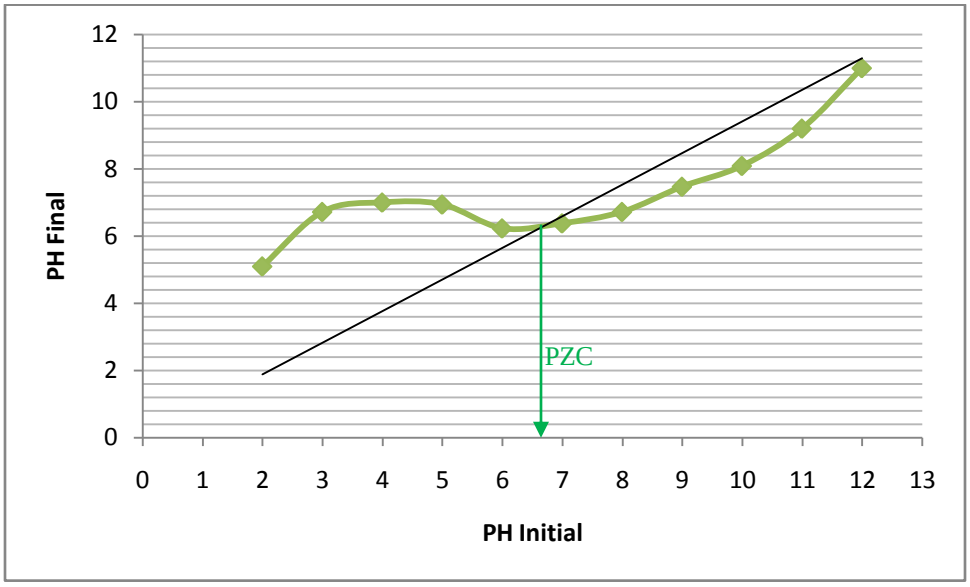

Figure D-4. A plot of pH_{Final} against $pH_{Initial}$ for the synthesized 40-ZnO/SiO_2 photocatalyst

APPENDIX E

PRELIMINARY PHOTOCATALYTIC ACTIVITY OF THE SYNTHESIZED ZnO AND ZnO/SiO_2 PHOTOCATALYSTS

It should be noted that at low concentration of the pollutants, the absorbance value (A) is equal to the concentration according to Beer- Lambert's law, since the parameters ε and L are constants. Therefore, Absorbance (A) = Concentration (C)

$$A=\log_{10}(I/I_0) = \varepsilon. C. L \qquad \text{E-1}$$

Photocatalytic Degradation of Methylene Blue (MB)

Initial concentration of methylene blue (MB) =10mg/L

Initial absorbance value of methylene blue (MB) = 1.412

Maximum wavelength (λmax) for MB absorption =665nm

Catalyst dosage= 0.1g/100ml of solution

Source of light = Solar irradiation

Dark absorption= 30 minutes

Initial concentration at time zero (t =0) using ZnO is: $C_0 = 1.243$

Initial concentration at time zero (t =0) using 20-ZnO/SiO_2 is: $C_0 = 1.398$

Initial concentration at time zero (t =0) using 30-ZnO/SiO_2 is: $C_0 = 1.389$

Initial concentration at time zero (t =0) using 40-ZnO/SiO_2 is: $C_0 = 1.370$

Degradation $(\%) = \frac{C_0 - C_t}{C_0}$ X 100%. E-2

Table E2: % degradation for photocatalytic degradation of MB using the synthesized photocatalysts

Time (min)	ZnO	20-ZnO/SiO_2	30-ZnO/SiO_2	40-ZnO/SiO_2
0.000	0.000	0.000	0.000	0.000
15.000	7.241	2.146	4.536	7.299
30.000	15.527	4.650	9.575	16.058
45.000	25.020	7.296	13.895	21.898
60.000	35.640	9.871	18.359	29.197
75.000	49.155	12.375	21.958	33.577
90.000	54.545	16.023	30.886	44.015

Table E3: $Ln\,{C_0}/{C_t}$ for photocatalytic degradation of MB using the synthesized photocatalysts

Time (min)	ZnO	20-ZnO/SiO_2	30-ZnO/SiO_2	40-ZnO/SiO_2
0.000	0.000000	0.000000	0.000000	0.000000
15.000	0.075161	0.021693	0.046417	0.075794
30.000	0.168738	0.047611	0.100652	0.175049
45.000	0.287950	0.075760	0.149601	0.247152
60.000	0.440671	0.103931	0.202833	0.345270
75.000	0.676394	0.132102	0.247926	0.409121
90.000	0.788457	0.174626	0.369406	0.580079

Photocatalytic Degradation of Benzoic acid (BA)

Initial concentration of benzoic acid (BA) = 20mg/L

Initial absorbance value of benzoic acid = 1.539

Maximum wavelength (λmax) for MB absorption =225nm

Catalyst dosage= 0.1g/100ml of solution

Source of light = Solar irradiation

Dark absorption= 30 minutes

Initial concentration at time zero (t =0) using ZnO is: C_0 = 1.428

Initial concentration at time zero (t =0) using 20-ZnO/SiO_2 is: C_0 = 1.531

Initial concentration at time zero (t =0) using 30-ZnO/SiO_2 is: C_0 = 1.522

Initial concentration at time zero (t =0) using 40-ZnO/SiO_2 is: C_0 = 1.505

Table E4: Absorbance test for photocatalytic degradation of BA using the synthesized photocatalysts.

Time (min)	ZnO	20-ZnO/SiO_2	30-ZnO/SiO_2	40-ZnO/SiO_2
0.000	1.428	1.531	1.522	1.505
15.000	1.278	1.467	1.400	1.358
30.000	1.121	1.402	1.320	1.209
45.000	0.982	1.398	1.224	1.066
60.000	0.825	1.263	1.133	0.918
75.000	0.636	1.190	1.048	0.769
90.000	0.489	1.148	0.963	0.620

Table E5: % degradation for photocatalytic degradation of BA using the synthesized photocatalysts

Time (min)	ZnO	20-ZnO/SiO_2	30-ZnO/SiO_2	40-ZnO/SiO_2
0.000	0.000	0.000	0.000	0.000
15.000	10.504	4.180	8.016	9.767
30.000	21.499	8.426	13.272	19.668
45.000	31.233	8.687	19.580	29.169
60.000	42.227	17.505	25.559	39.003
75.000	55.462	22.273	31.143	48.904
90.000	65.756	25.016	36.728	58.804

Table E6: $Ln\,{C_0}/{C_t}$ for photocatalytic degradation of BA using the synthesized photocatalysts

Time (min)	ZnO	20-ZnO/SiO_2	30-ZnO/SiO_2	40-ZnO/SiO_2
0.000	0.000000	0.000000	0.000000	0.000000
15.000	0.110979	0.042702	0.083553	0.10278
30.000	0.242054	0.088021	0.142394	0.218999
45.000	0.374439	0.090878	0.217901	0.344880
60.000	0.548647	0.192431	0.295156	0.494351
75.000	0.808832	0.251968	0.373142	0.671457
90.000	1.071668	0.287900	0.457727	0.886829

APPENDIX F

DETREMINATION OF PHYSICO – CHEMICAL PROPERTIES OF THE WASTE COOKING OIL

Saponification Value

$$SV = \frac{56.1 * C_{HCl} * (B - S)}{w} = \frac{56.1 * 0.5 * (B - S)}{w} = \frac{28.05 * (B - S)}{w} \quad \text{F-1}$$

Where B = titre value of the blank, S = titre value of the sample, w = weight of the oil, 56.1 = molecular mass of KOH, and C = concentration of HCl (0.5 mol/dm^3)

Titre values: $B_1 = 34.8cm^3$, $S_1 = 21.93cm^3$

$$SV_1 = \frac{28.05 * (34.8 - 21.93)}{2} = 180.50 mgKOH/g$$

Titre values: $B_2 = 34.5cm^3$, $S_2 = 21.66cm^3$

$$SV_2 = \frac{28.05 * (34.5 - 21.66)}{2} = 180.08 mgKOH/g$$

$$SV_{average} = \frac{180.50 + 180.08}{2} = 180.291 mgKOH/g$$

Acid Value

$$AV = \frac{56.1 * V * C}{w} \quad \text{F-2}$$

Where 56.1 = molecular mass of KOH

V = titre value of KOH solution used (cm^3)

C = concentration of the standard volumetric (KOH) solution used ($0.1mol/dm^3$)

w = mass of the test portion of the oil (g).

Titre values: $V_1 = 1.99cm^3$, $V_2 = 2.00cm^3$

$$V_{average} = \frac{1.99 + 2.00}{2} = 2.00cm^3$$

$$AV = \frac{56.1 * 2.00 * 0.1}{1} = 11.22mgKOH/g$$

$\% FFA = AV * 1.99^{-1} = 11.22 * 0.503 = 5.64\%$

Molecular Weight

$$M = \frac{56.1 * 1000 * 3}{SV - AV}$$

Where SV = Saponification value of the raw WCO

AV = Acid value of the raw WCO

$$M = \frac{56.1 * 1000 * 3}{180.29 - 11.22} = 995.45g/mol$$

APPENDIX G

DETERMINATION OF THE AMOUNT OF THE REACTANTS (WCO, METHANOL AND PHOTOCATALYST) FOR ESTERIFICATION REACTION

Basis: Methanol to WCO ratio (12:1), 100g of WCO

Mole of the WCO required = $\frac{mass\ of\ the\ WCO}{Molar\ mass\ of\ the\ WCO}$

$$n = \frac{100}{995.45} = 0.1\text{mole}$$

Number of moles of methanol required

0.1*12 = 1.2moles.

Therefore, amount of methanol required in gram is:

Mass (g) = number of moles * molar mass of methanol

1.2 *32.04 = **38.448g**

Amount of the photocatalyst required in gram is:

= 2%wt of the WCO

i.e. $\frac{2}{100}$ * 100 = **2g**

In summary,

The amounts of the reactants required for esterification reaction are:

WCO = 100g, Methanol = 38.448g, Photocatalyst = 2g

APPENDIX H

ESTERIFICATION RESULTS

$$\%C_{FFA} = \frac{A_i - A_t}{A_i} \text{ x } 100\% \qquad \text{H-1}$$

Where A_i = initial acid value of raw WCO (A_i = 11.22mgKOH/g), A_t = acid values of the esterified WCO after irradiation time.

It should be noted that:

I. Equation F-2 was used to determine the acid values of the esterified WCO

II. Equation H-1 was used to calculate percentage FFA conversion of the WCO after esterification reaction.

III. The distance between the light source and reaction vessel was fixed to be 40cm throughout the photochemical esterification process.

Photochemical Esterification (without the catalyst)

Table H-1: photochemical esterification result using 100W bulb

Mass of oil used (g)	Irradiation time (hr)	Titre value (cm^3)	Acid value (mgKOH/g)	$\%C_{FFA}$
1.20	1	V_1 = 2.26, V_2 = 2.30 V_{av} = 2.28	10.659	5.00
1.12	2	V_1 = 2.10, V_2 = 2.0 V_{av} = 2.05	10.268	8.48
1.04	3	V_1 = 1.79, V_2 = 1.73 V_{av} = 1.76	9.494	22.44
1.27	4	V_1 = 1.93, V_2 = 2.01 V_{av} = 1.97	8.702	22.44

Table H-2: photochemical esterification result using 200W bulb

Mass of oil used (g)	Irradiation time (hr)	Titre value (cm^3)	Acid value (mgKOH/g)	$\%C_{FFA}$
1.14	1	$V_1 = 2.15$, $V_2 = 1.99$ $V_{av} = 2.07$	10.187	9.21
1.08	2	$V_1 = 1.86$, $V_2 = 1.80$ $V_{av} = 1.83$	9.506	15.28
1.31	3	$V_1 = 1.81$, $V_2 = 1.85$ $V_{av} = 1.83$	7.837	30.15
1.25	4	$V_1 = 1.54$, $V_2 = 1.58$ $V_{av} = 1.56$	7.000	37.61

Table H-3: photochemical esterification result using 500W bulb

Mass of oil used (g)	Irradiation time (hr)	Titre value (cm^3)	Acid value (mgKOH/g)	$\%C_{FFA}$
1.20	1	$V_1 = 1.52$, $V_2 = 1.58$ $V_{av} = 1.55$	7.246	35.42
1.09	2	$V_1 = 1.24$, $V_2 = 1.28$ $V_{av} = 1.26$	6.485	42.20
1.03	3	$V_1 = 1.16$, $V_2 = 1.00$ $V_{av} = 1.08$	5.882	47.58
1.23	4	$V_1 = 1.09$, $V_2 = 1.11$ $V_{av} = 1.10$	5.017	55.29

Table H-4: Esterification of WCO using ZnO/SiO_2 catalysts in the dark for 6 hours

Supported catalysts	Mass of oil used (g)	Titre value (cm^3)	Acid value (mgKOH/g)	$\%C_{FFA}$
10-ZnO/SiO_2	1.06	$V_1 = 0.51$, $V_2 = 0.49$ $V_{av} = 0.50$	2.646	76.4
20-ZnO/SiO_2	1.12	$V_1 = 0.42$, $V_2 = 0.48$ $V_{av} = 0.45$	2.254	79.9
30-ZnO/SiO_2	1.08	$V_1 = 0.42$, $V_2 = 0.38$ $V_{av} = 0.40$	2.078	81.5
40-ZnO/SiO_2	1.55	$V_1 = 0.30$, $V_2 = 0.30$ $V_{av} = 0.30$	1.086	90.3

Table H-5: Photocatalytic esterification using SiO_2 as control experiment

Mass of oil used (g)	Irradiation time (hr)	Titre value (cm^3)	Acid value (mgKOH/g)	$\%C_{FFA}$
1.25	1	$V_1 = 0.97$, $V_2 = 1.03$ $V_{av} = 1.00$	4.488	60.0
1.32	2	$V_1 = 0.82$, $V_2 = 0.88$ $V_{av} = 0.85$	3.613	67.8
1.09	3	$V_1 = 0.57$, $V_2 = 0.63$ $V_{av} = 0.60$	3.088	72.5
1.03	4	$V_1 = 0.58$, $V_2 = 0.52$ $V_{av} = 0.55$	2.996	73.3

Table H-6: Photocatalytic esterification using the synthesized ZnO

Mass of oil used (g)	Irradiation time (hr)	Titre value (cm^3)	Acid value (mgKOH/g)	$\%C_{FFA}$
1.17	1	$V_1 = 0.27$, $V_2 = 0.23$ $V_{av} = 0.25$	1.199	89.3
1.09	2	$V_1 = 0.19$, $V_2 = 0.21$ $V_{av} = 0.20$	1.029	90.8
1.31	3	$V_1 = 0.22$, $V_2 = 0.18$ $V_{av} = 0.20$	0.856	92.4
1.12	4	$V_1 = 0.13$, $V_2 = 0.17$ $V_{av} = 0.15$	0.751	93.3

Table H-7: Photocatalytic esterification using 10 –ZnO/SiO_2

Mass of oil used (g)	Irradiation time (hr)	Titre value (cm^3)	Acid value (mgKOH/g)	$\%C_{FFA}$
1.00	1	$V_1 = 0.77$, $V_2 = 0.81$ $V_{av} = 0.79$	4.432	60.5
1.20	2	$V_1 = 0.81$, $V_2 = 0.75$ $V_{av} = 0.78$	3.647	67.5
1.25	3	$V_1 = 0.64$, $V_2 = 0.68$ $V_{av} = 0.66$	2.962	73.6
1.15	4	$V_1 = 0.46$, $V_2 = 0.52$ $V_{av} = 0.49$	2.390	78.7

Table H-8: Photocatalytic esterification using 20 –ZnO/SiO_2

Mass of oil used (g)	Irradiation time (hr)	Titre value (cm^3)	Acid value (mgKOH/g)	$\%C_{FFA}$
1.18	1	$V_1 = 0.78$, $V_2 = 0.84$ $V_{av} = 0.81$	3.851	65.7
1.07	2	$V_1 = 0.62$, $V_2 = 0.60$ $V_{av} = 0.61$	3.198	71.5
1.25	3	$V_1 = 0.59$, $V_2 = 0.55$ $V_{av} = 0.57$	2.558	77.2
1.00	4	$V_1 = 0.39$, $V_2 = 0.33$ $V_{av} = 0.36$	2.020	82.0

Table H-9: Photocatalytic esterification using 30 –ZnO/SiO_2

Mass of oil used (g)	Irradiation time (hr)	Titre value (cm^3)	Acid value (mgKOH/g)	$\%C_{FFA}$
1.02	1	$V_1 = 0.63$, $V_2 = 0.57$ $V_{av} = 0.60$	3.300	70.6
1.01	2	$V_1 = 0.50$, $V_2 = 0.50$ $V_{av} = 0.50$	2.777	75.3
1.06	3	$V_1 = 0.38$, $V_2 = 0.42$ $V_{av} = 0.40$	2.117	81.1
1.26	4	$V_1 = 0.40$, $V_2 = 0.40$ $V_{av} = 0.40$	1.781	84.1

Table H-10: Photocatalytic esterification using 40 –ZnO/SiO_2

Mass of oil used (g)	Irradiation time (hr)	Titre value (cm^3)	Acid value (mgKOH/g)	$\%C_{FFA}$
1.17	1	$V_1 = 0.30$, $V_2 = 0.30$ $V_{av} = 0.30$	1.439	87.2
1.05	2	$V_1 = 0.20$, $V_2 = 0.20$ $V_{av} = 0.20$	1.069	90.5
1.08	3	$V_1 = 0.19$, $V_2 = 0.15$ $V_{av} = 0.17$	0.883	92.1
1.17	4	$V_1 = 0.13$, $V_2 = 0.15$ $V_{av} = 0.14$	0.671	94.0

APPENDIX I

GC–MS RESULTS

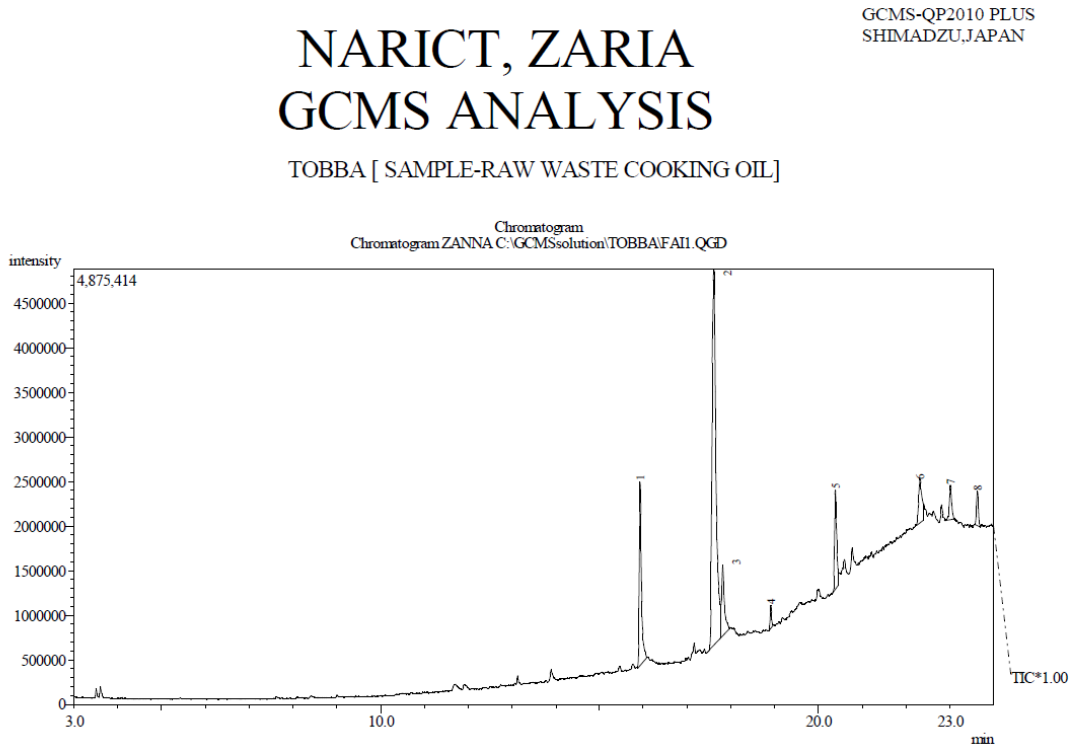

Figure I-1: GC –MS Chromatogram of the Waste Cooking Oil (WCO)

Table I-1: Peak Report of Waste Cooking Oil (WCO)

Peak#	R.Time	I.Time	F.Time	Area	Area%	Height	Height%	A/H
1	15.928	15.867	16.083	7456596	15.71	2053593	21.20	3.63
2	17.611	17.508	17.767	26784554	56.42	4208328	43.44	6.36
3	17.812	17.767	17.967	3594475	7.57	787749	8.13	4.56
4	18.912	18.867	18.967	606679	1.28	256658	2.65	2.36
5	20.381	20.325	20.458	3896521	8.21	1117494	11.54	3.49
6	22.318	22.233	22.392	2496074	5.26	492479	5.08	5.07
7	23.013	22.883	23.092	1421931	3.00	386736	3.99	3.68
8	23.627	23.567	23.700	1215116	2.56	384289	3.97	3.16
				47471946	100.00	9687326	100.00	

GCMS-QP2010 PLUS
SHIMADZU,JAPAN

NARICT, ZARIA
GCMS ANALYSIS

TOBBA [SAMPLE-DARK]

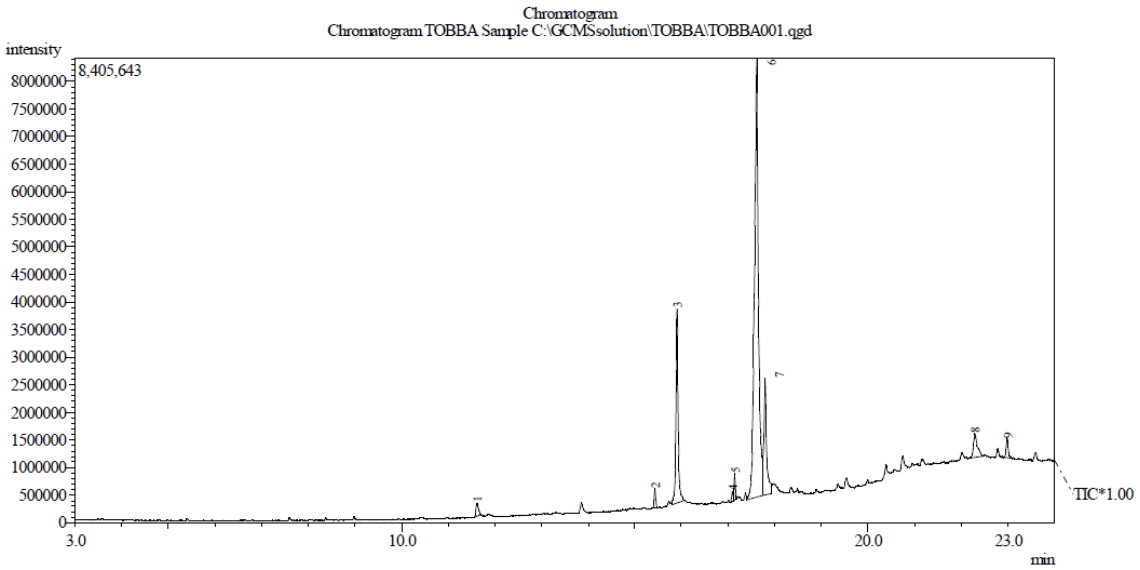

Figure I-2: GC –MS Chromatogram of the esterified WCO in the dark

Table I-2: Peak Report of the esterified WCO in the dark

Peak#	R.Time	I.Time	F.Time	Area	Area%	Height	Height%	A/H
1	11.618	11.558	11.700	910699	1.22	233041	1.49	3.91
2	15.434	15.383	15.483	741198	0.99	360568	2.31	2.06
3	15.907	15.783	16.067	12043569	16.15	3522295	22.57	3.42
4	17.091	17.050	17.108	346055	0.46	180914	1.16	1.91
5	17.142	17.108	17.183	936183	1.26	476813	3.06	1.96
6	17.615	17.400	17.750	47810508	64.10	7941888	50.89	6.02
7	17.792	17.750	17.933	8123148	10.89	2111135	13.53	3.85
8	22.293	22.200	22.467	2508821	3.36	427669	2.74	5.87
9	22.983	22.833	23.058	1163765	1.56	352689	2.26	3.30
				74583946	100.00	15607012	100.00	

GCMS-QP2010 PLUS
SHIMADZU,JAPAN

NARICT, ZARIA
GCMS ANALYSIS

TOBBA [SAMPLE-PHOTOESTERIFICATION]

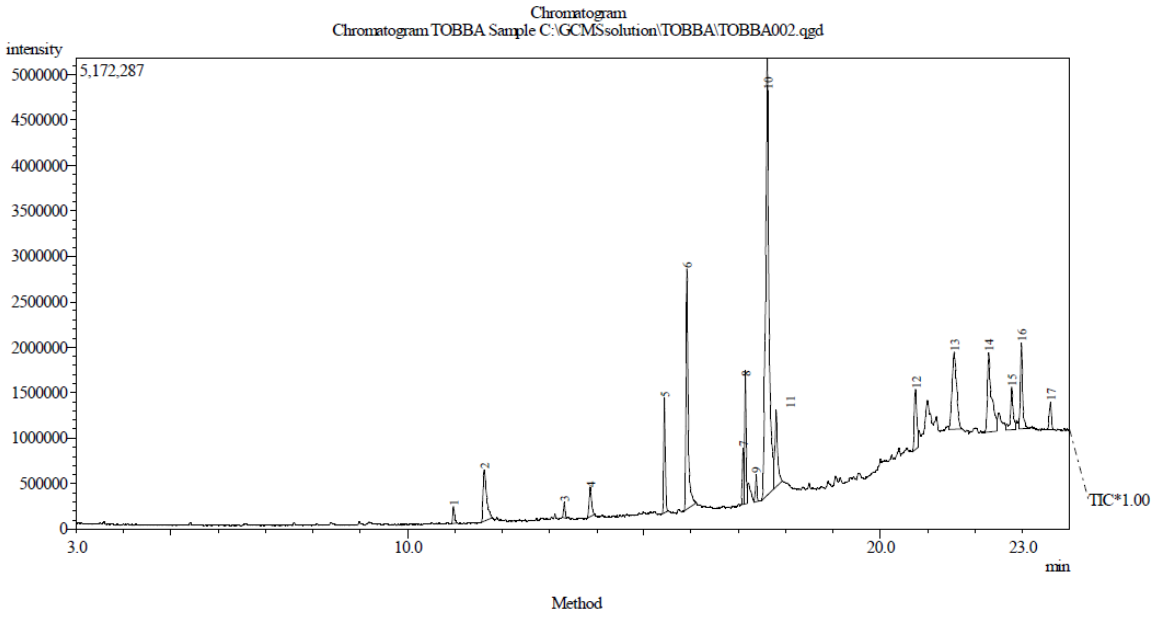

Figure I-3: GC –MS Chromatogram of the photocatalytic esterification of WCO

Table I-3: Peak Report for photocatalytic esterification of WCO

Peak#	R.Time	I.Time	F.Time	Area	Area%	Height	Height%	A/H
1	10.974	10.933	11.050	439291	0.64	190538	1.10	2.31
2	11.623	11.558	11.792	3013862	4.39	566778	3.28	5.32
3	13.313	13.275	13.367	347644	0.51	169344	0.98	2.05
4	13.861	13.808	13.958	1192561	1.74	328075	1.90	3.64
5	15.435	15.383	15.508	2727470	3.97	1266124	7.32	2.15
6	15.910	15.850	16.100	8739599	12.72	2641876	15.27	3.31
7	17.093	17.050	17.117	1333146	1.94	625568	3.62	2.13
8	17.144	17.117	17.183	3182754	4.63	1462402	8.45	2.18
9	17.368	17.317	17.417	633216	0.92	302799	1.75	2.09
10	17.608	17.483	17.750	24328776	35.42	4796399	27.72	5.07
11	17.793	17.750	17.925	3250477	4.73	854403	4.94	3.80
12	20.737	20.675	20.800	2350555	3.42	658589	3.81	3.57
13	21.559	21.450	21.708	5619930	8.18	847996	4.90	6.63
14	22.290	22.208	22.458	5398555	7.86	873222	5.05	6.18
15	22.775	22.642	22.858	2015129	2.93	468444	2.71	4.30
16	22.981	22.917	23.108	3212502	4.68	942105	5.45	3.41
17	23.591	23.542	23.667	905195	1.32	307233	1.78	2.95
				68690662	100.00	17301895	100.00	